Millimeter and submillimeter observations of the Orion Bar. I. Physical structure

Hogerheijde, M.R.; Jansen, D.J.; Dishoeck, E.F. van

Astron. Astrophys. 294, 792–810 (1995)

ASTRONOMY AND ASTROPHYSICS

Millimeter and submillimeter observations of the Orion Bar

I. Physical structure

Michiel R. Hogerheijde, David J. Jansen, and Ewine F. van Dishoeck

Sterrewacht Leiden, P.O. Box 9513, NL-2300 RA Leiden, The Netherlands

Received 30 May 1994 / Accepted 23 August 1994

Abstract. Millimeter and submillimeter observations of 53 rotational transitions of 18 different molecules and their isotopic varieties are presented at five positions on a strip crossing the Orion Bar. These data are used to study the physical and chemical conditions with increasing depth into the photon–dominated region (PDR). It is found that all molecules show about the same intensity distribution across the Bar. They peak $\sim 30''$ outside the ionization front, and fall off to about 10–20% of their peak values on either side. An excitation analysis of $C^{18}O$, H_2CO, CS and HCO^+ shows that the Orion Bar is best described by an inhomogeneous density distribution where $\sim$ 10% of the molecular material is comprised in clumps of hydrogen number density $n_{H_2} \approx 1^{+3.0}_{-0.7}\,10^6$ cm^{-3} and $\sim$ 90% in a homogeneous interclump medium of $n_{H_2} \approx 3^{+2.0}_{-2.2}\,10^4$ cm^{-3}. The kinetic temperature is found to be 85 ± 30 K. No significant variations in these physical parameters occur across the Bar. It is therefore concluded that the observed peak in the molecular rotational emission corresponds to a peak in molecular column densities. A geometric model for the Orion Bar is proposed in which with increasing distance from the ionizing stars, the PDR changes from a face–on to an edge–on geometry and back. The increased emission is then caused by the increased length of the line–of–sight through the PDR. This model is found to correspond well with other observations.

Key words: ISM: Orion Bar – ISM: molecules – ISM: structure – radio lines: ISM

1. Introduction

When a molecular cloud is illuminated by an intense far–ultraviolet radiation field, a so–called photon–dominated region (PDR) is created. The copious amounts of far–ultraviolet photons of young OB stars create an H II region in their immediate vicinity. Beyond the limit of this H II region, set by the penetration length of photons with an energy in excess of the 13.6 eV Lyman limit, a PDR is created in the transition zone to the parental molecular cloud.

The Orion Bar is a conspicuous example of a PDR. It is located approximately $2'$ south-east of the Trapezium stars and forms part of the larger Orion Molecular Cloud 1 (OMC–1 or Orion–A), which lies at a distance of approximately 450 pc. This cloud is the scene of massive star formation. The youngest of these stars form the Trapezium (θ^1 Ori) OB association, and are the ionizing source of the Orion Nebula H II region. The Orion Bar forms the sharp edge of the 6 cm continuum emission tracing the bulk of the H II region (Johnston et al. 1983). Just outside this ionization front, layers of enhanced atomic and molecular emission have been detected. For example, Boreiko et al. (1988) find strong [C II] 157.8 μm $^2P_{3/2} \rightarrow {}^2P_{1/2}$ fine–structure lines at the Orion Bar, whereas Stacey et al. (1993) have mapped OMC–1 in the [C II] 158 μm line and White & Padman (1991) in the [C I] 609 μm line. Strong [O I] 63 μm emission is found by Stacey et al. (1983) and [Si II] 35 μm by Haas et al. (1986). The presence of large amounts of warm, dense molecular gas ($n_{H_2} \geq 10^4$ cm^{-3}, $T_{kin} \approx$ 100 K) is indicated by ^{13}CO 6 $\rightarrow$ 5 and 3 $\rightarrow$ 2 observations of Graf et al. (1990), and ^{12}CO 7 $\rightarrow$ 6 and 14 $\rightarrow$ 13 data of Stacey et al. (1993).

Even higher temperature molecular gas up to $T \approx$2000 K is probed through the ro–vibrational transitions of H_2. Hayashi et al. (1985) report observations of vibrational emission of H_2 at nine positions at $14''$ intervals along a strip perpendicular to the Orion Bar. From comparison of the ratio of the H_2 $v = 1 \rightarrow 0$ S(1) and $v = 2 \rightarrow 1$ S(1) lines, and the integrated intensity of CS $J = 2 \rightarrow 1$ (Omodaka et al. 1984), they conclude that the gas at the molecular peak is shock excited, whereas that away from the peak is more fluorescently excited. Parmar et al. (1991) have made observations of low–J, pure rotational transitions of H_2 $v = 0$ $J = 3 \rightarrow 1$ and $4 \rightarrow 2$ (17 μm and 12 μm respectively) at eight positions on a northwest–southeast line across the Bar. They find that the emission of both lines peaks about $15''$ outside the ionization front and derive kinetic temperatures decreasing from $\sim$ 1000 K to $\sim$ 400 K with increasing depth into the cloud.

The observations of enhanced atomic and molecular emission in the PDR region are consistent with models of such regions developed e.g. by Tielens & Hollenbach (1985a), van

Send offprint requests to: M.R. Hogerheijde

Table 1. Telescopes: technical details

Telescope	Band	θ_{beam}	Beam efficiency	Resolution	Beam dilution η_c	
						$\Delta\alpha = 10''$
	GHz	$''$	η_{mb}	km s^{-1}	$\Delta\alpha = 15''$	$\Delta\alpha = 20''$
JCMT	230	21	0.65[a]	0.1, 0.4	0.82	0.86
	345	15	0.50	0.16	0.91	0.93
	492	11	0.37	0.31	0.92	0.94
CSO	230	32	0.72	0.60, 0.06	0.68	0.74
	345	20	0.60	0.40, 0.04	0.81	0.85
IRAM 30m	90	27	0.60	0.34	0.74	0.80
	140	17	0.59	0.21, 1.20, 2.30	0.87	0.90
	230	13	0.45	0.21, 1.20	0.92	0.94
NRAO 12m	140	44	1.0[b]	0.21	0.66	0.72

[a] Data obtained in August 1992 have $\eta_{mb} \simeq 0.53$, in April 1994 have $\eta_{mb} \simeq 0.70$.
[b] Spectra obtained at NRAO 12m are in T_R^* rather than T_A^*.

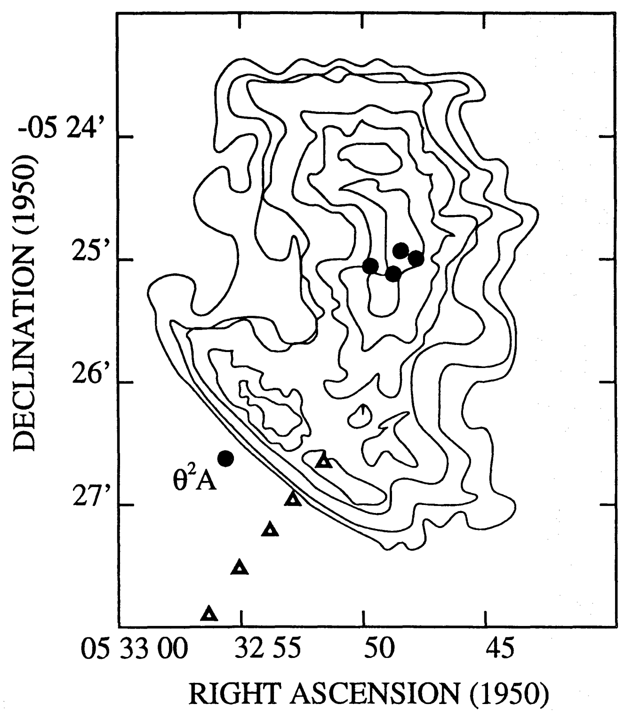

Fig. 1. Contour map of 6 cm continuum emission toward the Orion H II region (adapted from Johnston et al. 1983). The Orion Bar is delineated by the sharp ionization front in the southeast. The observed five positions are indicated with triangles. The positions of the Trapezium stars and θ^2A Ori are indicated with dots

Dishoeck & Black (1988), Sternberg & Dalgarno (1989), Burton et al. (1990), Le Bourlot et al. (1993), Meixner & Tielens (1993) and Köster et al. (1994) at various levels of sophistication. For the specific case of the Orion Bar, Tielens & Hollenbach (1985b) estimate that the radiation from the Trapezium stars corresponds to an enhancement over the average interstellar radiation field of a factor $\sim 4.4\ 10^4$. The star θ^2A Ori lies just south–east of the Orion Bar (outside the ionization front; see Fig. 1) and can contribute as well to the radiation field, having a spectral type O9.5. However, it is well known that the models, which apply to semi–infinite homogeneous slabs, fail to reproduce quantitatively the large observed amounts of warm CO (e.g. Graf et al. 1990; Graf et al. 1993), even with such high radiation fields. In order to solve this problem, it has been suggested that the PDR's have a clumpy structure, allowing the ultraviolet radiation to penetrate deeper into the cloud through the more diffuse interclump medium. Indeed, Tauber et al. (1994) have recently observed the Orion Bar at high angular resolution (6–10$''$) in ^{12}CO and ^{13}CO $J = 1 \rightarrow 0$ and HCO$^+$ $J = 1 \rightarrow 0$ using the BIMA (Berkeley Illinois Maryland Array) interferometer combined with FCRAO (Five College Radio Astronomy Observatory) single–dish data, and concluded that it consists of a homogeneous medium of $n_{H_2} \approx 5\ 10^4$ cm^{-3} with a small number of dense ($n_{H_2} > 10^6$ cm^{-3}) clumps dispersed throughout it (see also Tielens et al. 1993). These results, which became available after most of this work was completed, are quite consistent with the physical parameters found here (see Hogerheijde et al. 1994 for an earlier report).

Most previous observational studies of the Orion Bar have focussed on the atomic component, the distribution of the CO molecule in various transitions and the lowest (J = 1–0 or 2–1) millimeter lines of molecules with larger dipole moments such as HCO$^+$ and CS. However, for the high densities inferred for PDR's, the higher–lying submillimeter lines of these molecules are much more appropriate to constrain the physical structure. In addition, very little is known about the variation of molecular abundances across a PDR. The high spatial resolution offered by the submillimeter observations allows a detailed study of the chemical abundances in these regions. Since the Orion Bar PDR has been shown to be oriented almost perpendicular to the line–of–sight, it provides an excellent target to study the effect of the penetrating far–ultraviolet radiation on the physical parameters and chemical composition of the gas.

We have therefore performed millimeter and submillimeter observations of rotational lines of a large variety of molecular species toward five positions along a strip perpendicular to the

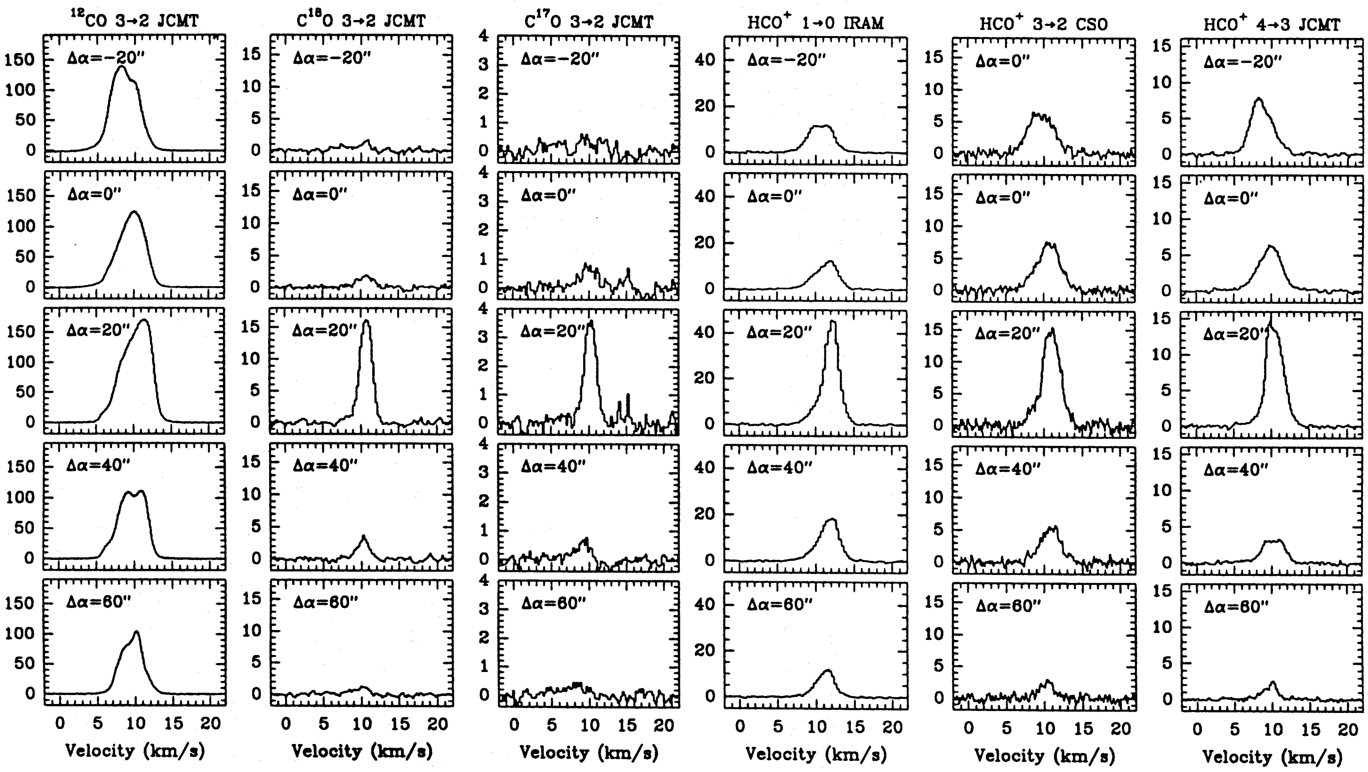

Fig. 2a. Observed spectra of ^{12}CO, $C^{18}O$, $C^{17}O$ and HCO^+ at the five positions toward the Orion Bar. Vertical scale is antenna temperature T_R in K, horizontal scale is V_{LSR} in km s^{-1}

Bar. We have chosen these positions from the original nine positions of Hayashi et al. (1985). They lie, in projection, in the H II region, at the ionization front, at the peak of the molecular emission and at increasing depth into the cloud (see Fig. 1). Our original motivation for choosing these positions was to also investigate the influence of shocks versus photons on the physical and chemical structure. However, as will be shown below, no evidence for the presence of strong shocks is found, contrary to the conclusion of Hayashi et al. (1985). Our aim is to derive from the observed transitions the H_2 number density, kinetic temperature and molecular column densities with increasing depth into the molecular cloud, and to devise a physical model explaining the observed characteristics. In a subsequent paper (Paper II, Jansen et al. 1994b) chemical modeling will be based on this model.

In Sects. 2 and 3, the observations are presented and the reduction methods discussed. In Sect. 4 the H_2 number density and kinetic temperature are derived using a homogeneous density model. We find such a model unable to explain the observed properties, and derive an inhomogeneous density model in Sect. 5. Molecular column densities are determined using the inferred density and temperature distributions. In Sect. 6 we propose a pure geometrical model explaining the observed characteristics of the Orion Bar.

2. Observations

From 1990 to 1994, 53 transitions of 18 different molecular species and some isotopic varieties were observed with the James Clerk Maxwell Telescope (JCMT)[1], the Caltech Submillimeter Observatory (CSO)[2], the Institut de Radio Astronomie Millimétrique (IRAM) 30m telescope and the National Radio Astronomy Observatory (NRAO) 12m telescope[3]. Table 1 summarizes the characteristics of the telescopes, such as their beam sizes at the observed frequencies and the velocity resolution of the backends used during the observations. The data were taken at five positions, 28″ apart, on the same strip almost perpen-

[1] The JCMT is operated by the Royal Observatory, Edinburgh, on behalf of the Particle Physics and Astronomy Research Council of the United Kingdom, the Netherlands Organization for Scientific Research and the National Research Council of Canada.

[2] The Caltech Submillimeter Observatory is operated by the California Institute of Technology under funding from the U.S. National Science Foundation (#AST90-15755)

[3] The National Radio Astronomy Observatory is operated by Associated Universities, Inc., under cooperative agreement with the U.S. National Science Foundation.

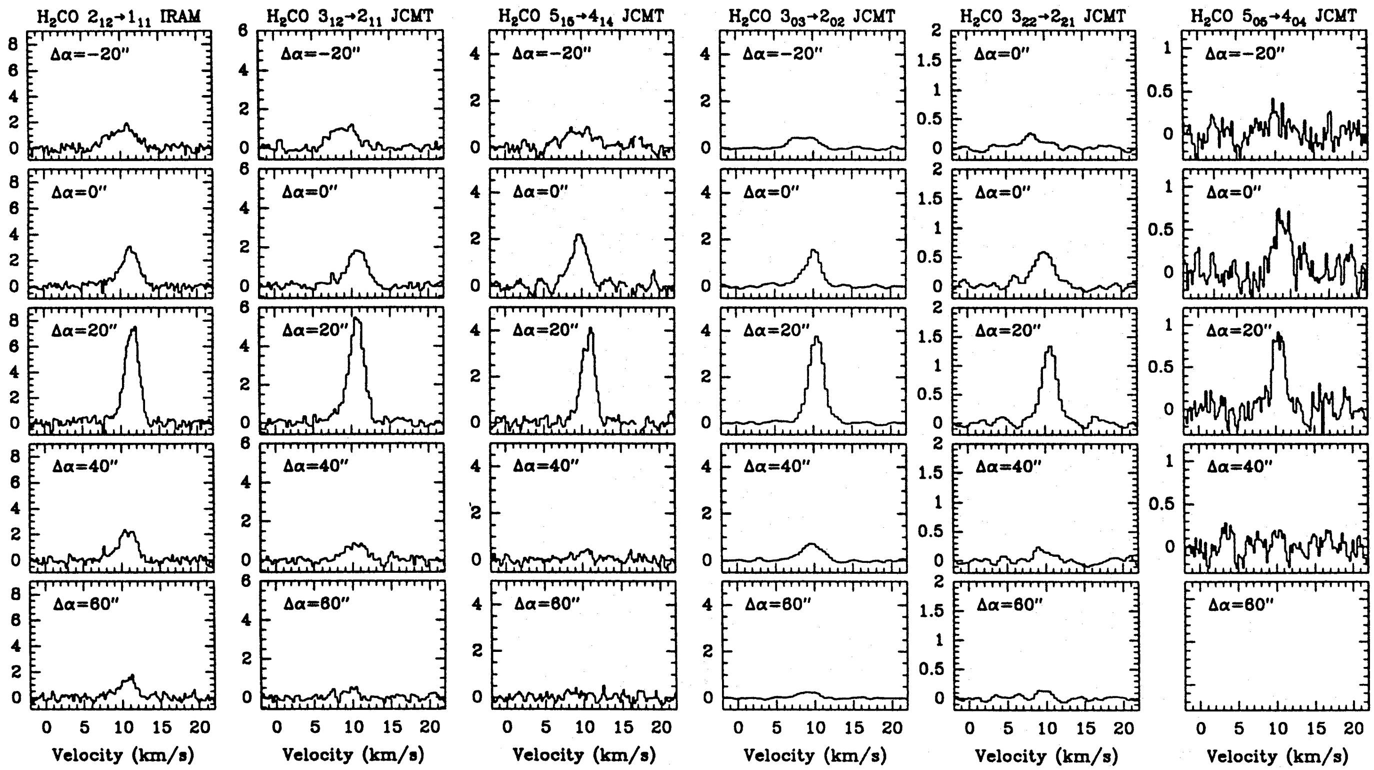

Fig. 2b. Observed spectra of H_2CO at the five positions toward the Orion Bar. Vertical scale is antenna temperature T_R in K, horizontal scale is V_{LSR} in km s^{-1}

dicular to the Orion Bar as used by Hayashi et al. (1985) (see Fig. 1). This spacing corresponds to one or two times the typical beam size, which varies from 14″ to 32″. The positions are designated by $(\Delta\alpha, \Delta\delta)$ with respect to $\alpha_{1950} = 5^h32^m52^s.7$ and $\delta_{1950} = -5°27'00''$ (the position of the ionization front), and have been chosen to coincide, in projection, with the H II region (−20″, 20″), the ionization front (0″, 0″), the peak of the molecular emission (20″, −20″) and with positions at increasing depth into the surrounding molecular cloud (40″, −40″) and (60″, −60″). Examples of spectra are presented in Fig. 2. In the following, the positions will be denoted by their $\Delta\alpha$ coordinate only.

The observations made with the JCMT and the CSO were obtained in double sideband mode, those at IRAM and NRAO in single sideband mode. It was assumed that either the sideband ratio was unity or that sideband cancellation was total. All observations were made in position switched mode, using an offset of +30′ in azimuth. A correction was made for the "flatfield" of the JCMT RxB3i receiver (350 GHz), which was found to have a varying response by ∼ 20% across its bandwidth (Baas, private communication).

To obtain information on the spatial extent of the emission, the strip across the Bar was sampled at less than half beam width intervals with steps of 5″ in $\Delta\alpha$ and $\Delta\delta$, in $C^{18}O$ 2 → 1 and SO $2_2 \rightarrow 1_1$ using the IRAM 30m telescope (Fig. 3). In addition, two maps of about 100″ × 100″ centered at the peak of the emission were made. The first is a fully sampled map (22″ spacing) in the H_2CO $2_{12} \rightarrow 1_{11}$ transition using the NRAO 12m (Fig. 4). The second, higher resolution map was obtained in the HCO^+ 3 → 2 transition using the JCMT. It was fully sampled (10″ spacing) around the region of the emission peak, and more sparsely sampled away from it (Fig. 5).

The observed antenna temperatures T_A^* are corrected for main beam efficiency using the factors listed in Table 1. From the fully sampled observations of $C^{18}O$ and SO along the strip and from the HCO^+ 3 → 2 map (see Sect. 3, Figs. 3 and 5), it is found that the emission has a peak with FWHM 20″ in $\Delta\alpha$ (i.e. 30″ on the sky) perpendicular to the Bar, but nearly constant intensity along the Bar. Thus, observations made with beams comparable to the width of the Bar or larger suffer from beam dilution, and the data have to be corrected for this effect before they can be combined with results obtained in different beams to determine line ratios. The estimated correction factors η_c for the various telescopes are included in Table 1, and were derived assuming Gaussian shapes for the telescope beams, and a Gaussian shape for the intensity distribution across the Bar. In doing so, it is assumed that all transitions show similar distributions, as is the case for $C^{18}O$, SO and HCO^+. The corrected

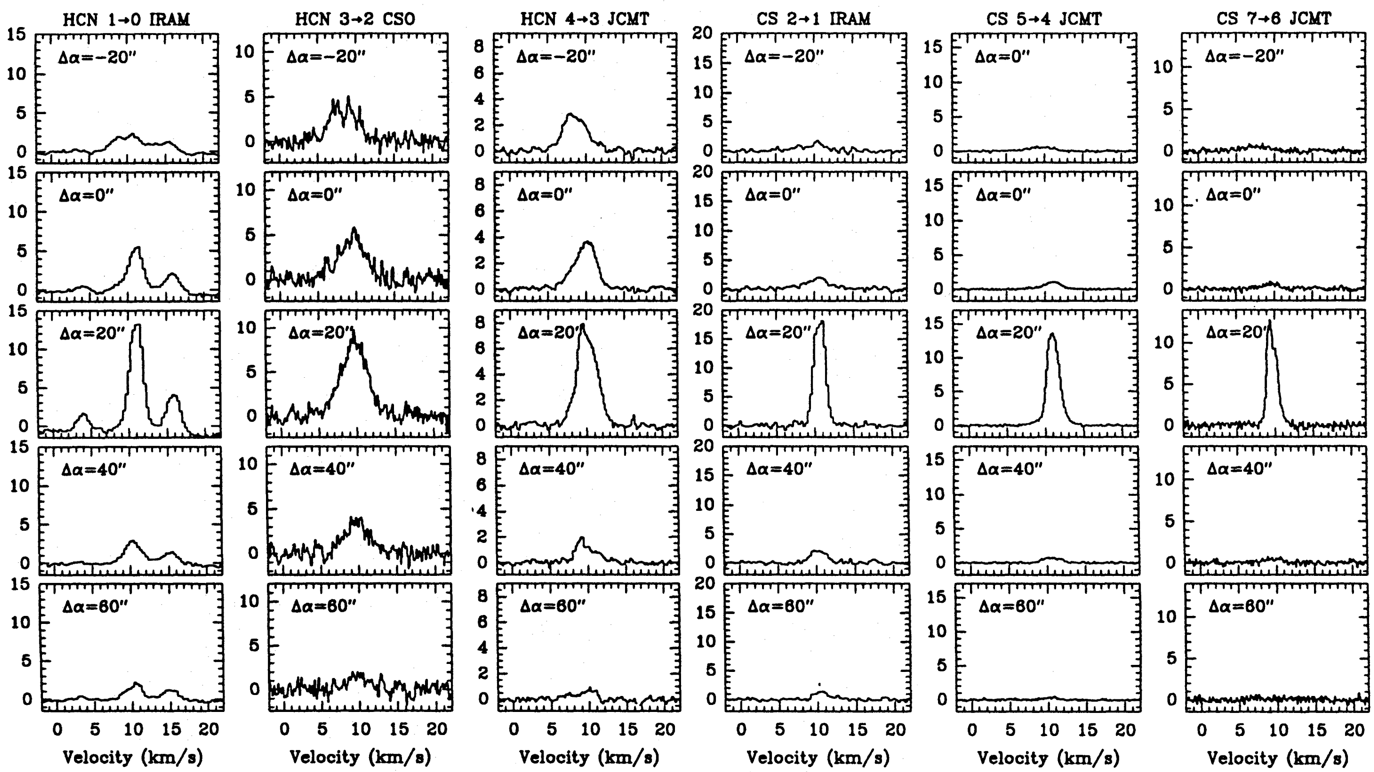

Fig. 2c. Observed spectra of HCN and CS at the five positions toward the Orion Bar. Vertical scale is antenna temperature T_R in K, horizontal scale is V_{LSR} in km s^{-1}

antenna temperatures correspond to T_R in the notation of Kutner & Ulich (1981). Because the beam sizes are of order 30″ or less, the applied corrections for beam dilution were no larger than 25%. Only observations at $\Delta\alpha$ = 10″, 15″ and 20″ have been corrected, since at greater distances from the peak, the intensity shows no variation on scales comparable to the beam sizes. This might underestimate the intensity at $\Delta\alpha$ = 0″ and 40″ somewhat, as some beams are large enough that they are still slightly sensitive to emission from the peak at these positions. However, the resulting errors are no larger than those due to other effects, e.g. small pointing errors (up to 5″ at the various telescopes).

The relative errors in T_R for transitions obtained with different telescopes or beam sizes are estimated to be about 30–40%, consisting of the error in the observations (10–20% for reasonable signal–to–noise), and the error in the correction factors for beam efficiency and beam dilution (20–30%). It is found that observations of the same transition at different occasions or with different telescopes agree to within this level. In Sects. 4 and 5 we will use the ratio of intensities, which have a relative error of 60% or less. If, however, observations made with the same beam size, or even within the same spectrum, are combined, the correction factor for beam dilution (and for beam efficiency) cancels, increasing the level of accuracy. On the other hand, at the positions $\Delta\alpha$ = +40″ and +60″, the signal–to–noise of the data is less, resulting in larger errors.

From the observed profiles presented in Fig. 2, it appears that two velocity components separated by about 1.5 km s^{-1} are present in the emitting gas, especially at the $\Delta\alpha$ = −20″ and 0″ positions. These two velocity components become more apparent in Fig. 4, where the contour map of the H_2CO $2_{12} \rightarrow 1_{11}$ emission is shown integrated over 5.0–9.0 km s^{-1} and 10.0–14.0 km s^{-1}, respectively. It is clear that the two components have very distinct spatial distributions, and that only the high velocity component is associated with the Bar. The low velocity component is attributed to a background (or foreground) cloud belonging to the Orion Ridge. This is consistent with the findings of e.g. Schloerb & Loren (1982) and Tauber et al. (1994). For some molecules (e.g. SO) only the component associated with the Bar appears to be present. Because of this, the derived width of the Orion Bar is not affected by the second component. Fits to the profiles of these molecules give V_{LSR}=10.3±0.4 km s^{-1} and a FWHM ΔV = 1.8 ± 0.3 km s^{-1}. These parameters for the Bar component were subsequently used to fit the profiles of other species, resulting in the parameters $V_{LSR} \approx 9$ km s^{-1} and $\Delta V \approx 3.5$ km s^{-1} for the background cloud component. It appeared that most spectra could be fit consistently with these two sets of parameters, the major exceptions being ^{12}CO, HCO^+

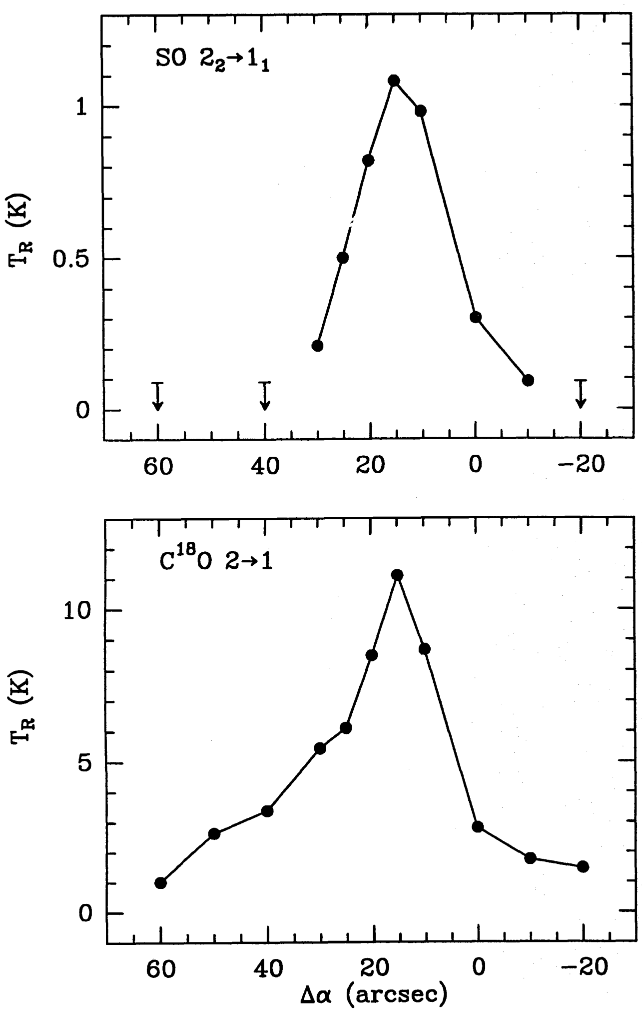

Fig. 3. Intensity distribution of SO $2_2 \rightarrow 1_1$ (top) and $C^{18}O$ 2 → 1 (bottom) observed in steps of 5″ in both $\Delta\alpha$ and $\Delta\delta$. Data were obtained with the IRAM 30m telescope. The Trapezium stars lie to the right side of each plot. From these observations a FWHM of ~ 30″ is derived for the brightness distribution of the Bar. The $C^{18}O$ distribution also shows emission from the background OMC–1 at positions away from the peak

and HCN (see below). The $C^{18}O$ 2 → 1 (Fig. 3) shows an additional underlying, more broadly distributed component at $V_{LSR} \simeq 10$ km s^{-1} due to the OMC–1. This cloud does not affect the emission in other lines (see Sect. 5.2).

3. Results

In Table 2 the parameters of the Gaussian fits to the data for the component at $V_{LSR} \approx 10.3$ km s^{-1} associated with the Orion Bar are presented. In Fig. 6 the observed T_R are shown, normalized to their value at the peak position. It is seen that most transitions have similar intensity distributions. They peak at (20″, −20″), and fall off to about 10% of their peak value at the outer positions. There are a few exceptions to this behavior. The ^{12}CO 3 → 2 intensity shows only a relatively small enhancement at the peak position, and its line profile is much broader than that of any other species (4–5 km s^{-1} as opposed to 2–4 km s^{-1}). This is probably caused by the fact that the Bar is optically thick at this transition due to the large abundance of ^{12}CO. This line can therefore be used as an indicator of the kinetic temperature T_{kin} of the gas (see Sect. 4).

Other exceptions are HCN 3 → 2 and 4 → 3, and HCO^+ 3 → 2 and 4 → 3. While their profiles can be fit in the usual way with two Gaussians at positions offset from the emission peak, their profiles at (20″, −20″) cannot. Also, the peak in their intensity distribution across the Bar is slightly less pronounced. This is again most likely caused by the fact that the gas is optically thick for these transitions at the peak position, so that for this position only the parameters of single Gaussian fits are listed in the table. It will later be shown in Sect. 5 that according to the model derived from the other lines, the cloud is indeed somewhat optically thick in these transitions at this position. This is also supported by the detection of $H^{13}CO^+$ 3 → 2.

It is assumed here that the contribution of any possible error beam of the telescopes is negligible. Considerable power in an error beam with an extent larger than 30″ would reproduce the observed low level emission at $\Delta\alpha \neq 20''$ by picking up emission from the peak. The similarity of intensity distributions obtained with different telescopes suggests that the observed distributions are not caused by an instrumental effect. Recent measurements of the JCMT beam shape at 240 GHz shows that the response outside the main beam is less than 2% of that of the main beam (Sandell, private communication).

The fact that higher excitation lines of simple molecules such as CS 7 → 6, H_2CO $5_{15} \rightarrow 4_{14}$, HCO^+ 4 → 3 and HCN 4 → 3 are readily detected at various positions across the Bar indicates that densities of the order of 10^6 cm^{-3} are present. The highest excitation line observed is the H_2CO $7_{17} - 6_{16}$ transition at 491.969 GHz for which the JCMT spectrum presented in Fig. 7 shows a 2σ feature. The critical density of this transition is about 3 10^7 cm^{-3}. In terms of the chemistry, a large number of other molecules have been detected at one or more positions toward the Orion Bar, including C_2H, CN, HNC, CH_3OH, SO and SO_2. Particularly interesting is the detection of H_2S in this PDR (see Jansen et al. 1994a) and that of CO^+, for which the first identification in the interstellar medium has only recently been reported by Latter et al. (1993) in the PDR M17SW and the planetary nebula NGC 7027. Undetected at a noise level of 0.10 K or less are higher–lying transitions of $H_2{}^{13}CO$, CH_3CCH, DCN, HNCO, CH_3CN, and SiO. More details about these species will be presented in Paper II (Jansen et al. 1994b).

4. Excitation analysis

The excitation analysis of the Orion Bar has been based primarily on the transitions of CS, $C^{18}O$, HCO^+ and H_2CO. For these molecules, the observed lines are optically thin and have high enough signal–to–noise at the five positions. An exception may be CS at $\Delta\alpha$=20″, where the observed ratio CS/$C^{34}S \approx 10 \pm 2$, suggesting an optical depth of about unity for the 5 → 4 transition. In Sect. 5.2 it will be shown that all included lines are

Table 2. Parameters of Gaussian fits to the observed profiles

			$\Delta\alpha = -20''$			$\Delta\alpha = 0''$			$\Delta\alpha = 20''$			$\Delta\alpha = 40''$			$\Delta\alpha = 60''$		
Molecule Transition	Frequency MHz	Telescope	ΔV km s^{-1}	T_R K	$\int T_R dV$ K km s^{-1}	ΔV km s^{-1}	T_R K	$\int T_R dV$ K km s^{-1}	ΔV km s^{-1}	T_R K	$\int T_R dV$ K km s^{-1}	ΔV km s^{-1}	T_R K	$\int T_R dV$ K km s^{-1}	ΔV km s^{-1}	T_R K	$\int T_R dV$ K km s^{-1}
$^{12}CO\ 3 \rightarrow 2$	345796	JCMT–94	2.4	78.6	198.8	2.8	64.4	191.2	2.0	108.8	236.0	1.5	63.0	100.0	1.8	35.2	67.6
$C^{18}O\ 2 \rightarrow 1$	219560	IRAM–92	1.7	1.46	2.59	2.1	2.81	6.23	1.8	8.48	16.1	1.8	3.38	6.46	1.8	1.01	1.93
$C^{18}O\ 3 \rightarrow 2$	329331	JCMT–92	1.6	1.26	2.19	1.8	1.40	2.67	1.9	15.3	30.2	1.8	2.84	5.41	1.8	0.80	1.54
$C^{17}O\ 3 \rightarrow 2$	337061	JCMT–92	–	< 2.0	–	1.8	0.56	1.08	1.8	3.63	6.97	–	< 0.2	–	–	< 0.2	–
$HCO^+\ 1 \rightarrow 0$	89189	IRAM–91	1.8	2.25	4.32	1.8	5.08	9.86	1.5	27.5	45.0	2.2	11.5	27.4	2.0	7.00	14.8
$HCO^+\ 3 \rightarrow 2$	267558	CSO–90	1.8	0.40	0.76	1.8	1.54	2.94	2.6	11.4	31.2	1.8	2.68	5.14	1.8	2.22	4.22
$HCO^+\ 4 \rightarrow 3$	356734	JCMT–92	–	< 1.0	–	1.8	1.31	2.52	2.7	13.1	37.6	1.5	1.42	2.32	1.8	1.78	3.42
$H^{13}CO^+\ 3 \rightarrow 2$	260255	JCMT–93	–	–	–	–	–	–	1.8	0.70	1.37	–	–	–	–	–	–
$H_2CO\ 2_{12} \rightarrow 1_{11}$	140840	IRAM–91	1.8	0.55	1.05	1.8	2.21	4.24	1.8	7.09	13.6	1.8	1.58	3.02	1.8	1.17	2.26
$H_2CO\ 3_{12} \rightarrow 2_{11}$	225698	JCMT–92	1.8	0.24	0.46	1.8	0.49	0.94	1.8	4.38	8.41	1.8	0.30	0.57	1.8	0.26	0.51
$H_2CO\ 5_{15} \rightarrow 4_{14}$	351769	JCMT–92	–	< 0.2	–	1.8	1.75	3.37	1.8	3.73	7.13	1.8	0.32	0.61	–	< 0.2	–
$H_2CO\ 7_{17} \rightarrow 6_{16}$	491969	JCMT–94[a]	–	–	–	–	–	–	1.5	1.51	2.49	–	–	–	–	–	–
$H_2CO\ 3_{03} \rightarrow 2_{02}$	218222	JCMT–93	1.8	0.09	0.18	1.8	1.18	2.25	1.8	3.47	6.65	1.8	0.15	0.30	1.8	0.13	0.25
$H_2CO\ 3_{22} \rightarrow 2_{21}$	218476	JCMT–92	1.8	0.08	0.13	1.8	0.71	1.36	1.8	1.55	2.97	1.8	0.30	0.57	–	< 0.08	–
$H_2CO\ 3_{22} \rightarrow 2_{21}$	218476	JCMT–93	–	–	–	1.8	0.32	0.62	1.8	1.24	2.37	–	< 0.05	–	–	–	—
$H_2CO\ 3_{21} \rightarrow 2_{20}$	218760	JCMT–93	–	< 0.08	–	1.8	0.82	1.57	1.8	1.41	2.70	–	< 0.08	–	–	< 0.08	–
$H_2CO\ 5_{05} \rightarrow 4_{04}$	362736	JCMT–92†	–	< 0.13	–	1.8	0.58	1.10	1.8	0.87	1.68	–	< 0.13	–	–	< 0.13	–
$H_2{}^{13}CO\ 3_{12} \rightarrow 2_{11}$	219909	JCMT–92	–	–	–	–	< 0.10	–	–	–	–	–	–	–	–	–	–
$HCN\ 1 \rightarrow 0$	88632	IRAM–91	1.8	1.32	2.52	1.8	3.94	7.52	1.8	11.2	21.4	1.8	1.03	1.97	1.8	0.82	1.56
$HCN\ 3 \rightarrow 2$	265886	CSO–90	–	< 1.0	–	–	< 1.0	–	3.5	6.2	23.0	1.8	1.21	2.31	–	< 1.0	–
$HCN\ 4 \rightarrow 3$	354505	JCMT–92	1.8	0.40	0.74	1.8	1.54	2.96	3.1	6.9	22.7	–	–	–	1.8	0.48	0.92
$CS\ 2 \rightarrow 1$	97981	IRAM–91	1.8	0.82	1.57	1.8	1.02	1.95	1.8	17.9	30.6	1.8	1.90	3.63	1.8	1.27	2.43
$CS\ 3 \rightarrow 2$	146969	IRAM–91	3.2[d]	0.39[d]	1.34	3.2[d]	0.64[d]	2.16	3.2[d]	10.9[d]	36.7	3.2[d]	1.93[d]	6.56	3.2[d]	0.51[d]	1.75
$CS\ 5 \rightarrow 4$	244936	JCMT–94	1.8	0.09	0.17	1.8	0.83	1.57	1.8	14.0	27.2	1.8	0.89	1.89	1.8	0.37	0.71
$CS\ 7 \rightarrow 6$	342883	JCMT–94	–	< 0.2	–	1.8	0.44	0.84	1.5	12.1	18.1	1.8	0.54	1.04	–	< 0.2	–
$C^{34}S\ 5 \rightarrow 4$	241016	JCMT–92	–	–	–	–	< 0.14	–	1.8	1.23	2.38	–	< 0.14	–	–	–	–
$C_2H\ 4_5 \rightarrow 3_4$	349338	JCMT–92[b]†	–	< 0.25	–	1.8	1.23	2.35	1.8	1.42	2.71	1.8	0.52	0.99	1.8	0.29	0.55
$C_2H\ 4_4 \rightarrow 3_3$	349399	JCMT–92[b]†	–	< 0.25	–	1.8	0.95	1.81	1.8	1.28	2.44	1.8	0.29	0.55	–	< 0.25	–

Table 2. (continued)

			$\Delta\alpha = -20''$			$\Delta\alpha = 0''$			$\Delta\alpha = 20''$			$\Delta\alpha = 40''$			$\Delta\alpha = 60''$		
Molecule Transition	Frequency MHz	Telescope	ΔV km s^{-1}	T_R K	$\int T_R dV$ K km s^{-1}	ΔV km s^{-1}	T_R K	$\int T_R dV$ K km s^{-1}	ΔV km s^{-1}	T_R K	$\int T_R dV$ K km s^{-1}	ΔV km s^{-1}	T_R K	$\int T_R dV$ K km s^{-1}	ΔV km s^{-1}	T_R K	$\int T_R dV$ K km s^{-1}
$CH_3OH\ 5_0 \rightarrow 4_0\ A^+$	241791	JCMT–92	–	–	–	–	< 0.06	–	1.8	0.62	0.91	–	< 0.06	–	–	< 0.06	–
$CH_3OH\ 5_1 \rightarrow 4_1\ E^-$	241767	JCMT–92	–	–	–	–	< 0.05	–	1.7	0.82	0.99	–	< 0.05	–	–	< 0.05	–
$CH_3OH\ 1_1 \rightarrow 0_0\ A^+$	350905	CSO–94[a]	–	–	–	–	–	–	5.0[d]	0.13[d]	0.75	–	–	–	–	–	–
$CH_3CCH\ 20_0 \rightarrow 19_0$	341741	JCMT–92	–	–	–	–	< 0.09	–	–	–	–	–	–	–	–	–	–
$CN\ 2_{\frac{3}{2}\frac{5}{2}} \rightarrow 1_{\frac{3}{2}\frac{5}{2}}$	226360	JCMT–92	–	–	–	1.8	0.57	1.09	1.8	0.81	1.5	–	< 0.14	–	–	–	–
$CN\ 3_{\frac{5}{2}} \rightarrow 2_{\frac{3}{2}}$	340035	JCMT–92[c]	–	< 0.2	–	1.8	1.05	2.00	1.8	3.47	6.62	1.8	0.30	0.57	1.8	0.37	0.71
$CN\ 3_{\frac{7}{2}} \rightarrow 2_{\frac{5}{2}}$	340248	JCMT–92[c]	–	< 0.2	–	1.8	2.14	4.08	1.8	7.83	15.0	1.8	0.25	0.48	–	< 0.2	–
$HNC\ 1 \rightarrow 0$	90664	IRAM–92	1.8	0.55	1.05	1.8	2.66	5.10	1.8	5.53	10.6	1.8	2.00	3.83	1.8	1.40	2.69
$HNC\ 4 \rightarrow 3$	362630	JCMT–92†	–	< 0.1	–	1.8	0.81	1.55	1.8	1.05	2.01	–	< 0.1	–	–	–	–
$DCN\ 5 \rightarrow 4$	362046	JCMT–92	–	–	–	–	< 0.06	–	–	–	–	–	–	–	–	–	–
$HNCO\ 6_{06} \rightarrow 5_{05}$	131886	IRAM–92	–	< 0.04	–	–	< 0.04	–	–	< 0.04	–	–	< 0.04	–	–	< 0.04	–
$CH_3CN\ 13_K \rightarrow 12_K$	239200	JCMT–92	–	–	–	–	< 0.05	–	–	< 0.05	–	–	–	–	–	–	–
$NO\ \frac{7}{2}\frac{9}{2} \rightarrow \frac{5}{2}\frac{7}{2}$	351043	CSO–94[a]	–	–	–	–	–	–	3.0[d]	0.20[d]	0.65	–	–	–	–	–	–
$NO\ \frac{7}{2}\frac{7}{2} \rightarrow \frac{5}{2}\frac{5}{2}$	351051	CSO–94[a]	–	–	–	–	–	–	2.4[d]	0.30[d]	0.78	–	–	–	–	–	–
$SO\ 2_2 \rightarrow 1_1$	86094	IRAM–92	–	< 0.09	–	2.0	0.30	0.63	2.0	0.82	1.75	–	< 0.09	–	–	< 0.09	–
$SO\ 6_5 \rightarrow 5_4$	219949	JCMT–92	–	–	–	1.6	0.64	1.09	1.9	5.81	11.8	1.6	0.33	0.56	–	–	–
$SO\ 8_8 \rightarrow 7_7$	344311	CSO–92	–	–	–	2.0	0.47	1.00	1.9	1.49	3.00	–	–	–	–	–	–
$SO\ 9_8 \rightarrow 8_7$	346528	JCMT–92†	–	< 0.2	–	–	< 0.2	–	1.8	1.82	3.50	–	< 0.2	–	–	< 0.2	–
$SO_2\ 5_{24} \rightarrow 4_{13}$	241616	IRAM–92	–	–	–	–	< 0.05	–	1.9	0.33	0.69	–	< 0.05	–	–	< 0.05	–
$H_2S\ 1_{10} \rightarrow 1_{01}$	168763	IRAM–92	1.8	0.43	0.81	1.8	4.85	9.29	1.8	18.8	36.0	1.8	2.68	5.12	–	< 0.5	–
$SiO\ 8 \rightarrow 7$	347331	JCMT–92	–	–	–	–	< 0.12	–	–	< 0.12	–	–	–	–	–	–	–
$CO^+\ 2_{\frac{3}{2}} \rightarrow 1_{\frac{1}{2}}$	235790	CSO–92[a]	–	–	–	–	–	–	1.8	0.13	0.25	–	–	–	–	–	–
$CO^+\ 2_{\frac{5}{2}} \rightarrow 1_{\frac{3}{2}}$	236063	CSO–92[a]	–	–	–	–	–	–	1.8	0.16	0.31	–	–	–	–	–	–
$CO^+\ 3_{\frac{7}{2}} \rightarrow 2_{\frac{5}{2}}$	354014	CSO–94[a]	–	–	–	–	–	–	4.0[d]	0.18[d]	0.75	–	–	–	–	–	–
$CO^+\ 3_{\frac{5}{2}} \rightarrow 2_{\frac{3}{2}}$	353741	CSO–94[a]	–	–	–	–	–	–	3.5[d]	0.13[d]	0.52	–	–	–	–	–	–
$C\,\textsc{i}\ 1 \rightarrow 0$	492161	JCMT–94[a]	–	–	–	–	–	–	2.5[d]	7.05[d]	19.1	–	–	–	–	–	–

† Possible pointing offset.
[a] Spectrum obtained at $\Delta\alpha = 15''$.
[b] $C_2H\ 4_5 \rightarrow 3_4$ and $4_4 \rightarrow 3_3$ doublet fit assuming relative contributions 1 : 0.08 and 1 : 0.74 respectively.
[c] $CN\ 3_{\frac{5}{2}} \rightarrow 2_{\frac{3}{2}}$ and $3_{\frac{7}{2}} \rightarrow 2_{\frac{5}{2}}$ doublet fit assuming equal contributions for all components.
[d] Unresolved lines: profiles are dominated by instrumental broadening.

Table 3. Results of homogeneous models

Transition	Telescopes	Ratio T_R/T_R					n_{H_2} (cm^{-3})				
	$\Delta\alpha$ =	−20″	0″	20″	40″	60″	−20″	0″	20″	40″	60″
$C^{18}O$ $3 \rightarrow 2/2 \rightarrow 1$	JCMT/IRAM	0.86	0.50	1.79	0.84	0.79	$1\,10^4$	$1\,10^4$	$>3\,10^4$	$1\,10^4$	$1\,10^4$
CS $7 \rightarrow 6/5 \rightarrow 4$	JCMT/JCMT	<2.39	0.53	0.87	0.61	<0.54	–	$1\,10^6$	$3\,10^6$	$2\,10^6$	$<2\,10^6$
CS $7 \rightarrow 6/3 \rightarrow 2$	JCMT/IRAM	<0.28	0.39	0.49	0.16	<0.21	$<1\,10^6$	$1\,10^6$	$1\,10^6$	$8\,10^5$	$<1\,10^6$
CS $7 \rightarrow 6/2 \rightarrow 1$	JCMT/IRAM	<0.22	0.43	0.68	0.26	<0.19	$<1\,10^6$	$1\,10^6$	$1\,10^6$	$1\,10^6$	$<1\,10^6$
CS $5 \rightarrow 4/3 \rightarrow 2$	JCMT/IRAM	0.12	0.72	0.74	0.29	0.41	$<5\,10^4$	$8\,10^5$	$8\,10^5$	$2\,10^5$	$5\,10^5$
CS $5 \rightarrow 4/2 \rightarrow 1$	JCMT/IRAM	0.10	0.81	0.77	0.46	0.29	$6\,10^4$	$1\,10^6$	$1\,10^6$	$6\,10^5$	$3\,10^5$
CS $3 \rightarrow 2/2 \rightarrow 1$	IRAM/IRAM	0.85	1.11	1.02	1.81†	0.72	$2\,10^5$	$4\,10^5$	$3\,10^5$	$>1\,10^6$	$2\,10^5$
H_2CO $7_{17} \rightarrow 6_{16}/5_{15} \rightarrow 4_{14}$	JCMT/JCMT[a]	–	–	<0.43	–	–	–	–	$<1\,10^7$	–	–
H_2CO $5_{15} \rightarrow 4_{14}/3_{12} \rightarrow 2_{11}$	JCMT/JCMT	<0.83	1.8	0.83	1.07	<0.77	$<2\,10^6$	$>1\,10^7$	$2\,10^6$	$3\,10^6$	$<2\,10^6$
H_2CO $5_{15} \rightarrow 4_{14}/2_{12} \rightarrow 1_{11}$	JCMT/IRAM	<0.36	0.79	0.52	0.20†	<0.17†	$<1\,10^5$	$8\,10^5$	$<1\,10^6$	$<1\,10^6$	$<1\,10^6$
H_2CO $3_{12} \rightarrow 2_{11}/2_{12} \rightarrow 1_{11}$	JCMT/IRAM	0.44	0.22†	0.63	0.19†	0.22†	$1\,10^5$	10^4–10^5	$3\,10^5$	10^4–10^5	10^4–10^5
H_2CO $5_{05} \rightarrow 4_{04}/3_{22} \rightarrow 2_{21}$	JCMT/JCMT(92)	<1.3	0.65	0.55	<0.34†	–	$1\,10^6$	$1\,10^5$	$1\,10^5$	–	–
H_2CO $5_{05} \rightarrow 4_{04}/3_{21} \rightarrow 2_{20}$	JCMT/JCMT	–	0.56	0.60	<1.7	–	–	$3\,10^5$	$3\,10^5$	$<1\,10^6$	–
H_2CO $5_{05} \rightarrow 4_{04}/3_{03} \rightarrow 2_{02}$	JCMT/JCMT	<1.4	0.49	0.25	<0.9	<1.0	$<1\,10^7$	$1\,10^6$	$3\,10^5$	$<3\,10^6$	$<3\,10^6$
H_2CO $3_{22} \rightarrow 2_{21}/3_{03} \rightarrow 2_{02}$	JCMT/JCMT(93)	0.26‡	0.27	0.37	<0.33	0.27‡	$>5\,10^3$	$>5\,10^3$	$>5\,10^3$	$>5\,10^3$	$>5\,10^3$
HCO^+ $4 \rightarrow 3/1 \rightarrow 0$	JCMT/IRAM	<0.50	0.26	–	0.12	0.25	$<1\,10^5$	$1\,10^5$	–	$5\,10^4$	$1\,10^5$
HCO^+ $4 \rightarrow 3/3 \rightarrow 2$	JCMT/CSO	<2.5	0.85	–	0.53	0.80	–	$1\,10^6$	–	$1\,10^5$	$1\,10^6$
HCO^+ $3 \rightarrow 2/1 \rightarrow 0$	CSO/IRAM	0.18	0.30	–	0.23	0.32	$3\,10^4$	$3\,10^4$	–	$3\,10^4$	$3\,10^4$

† Ratio uncertain due to bad fit to one of the lines.
‡ Ratio of integrated intensities uncertain because of poor quality of spectrum. Includes contribution o second velocity component.
[a] Ratio of measurements at $\Delta\alpha$ = 15″ and $\Delta\alpha$ = 20″.

indeed effectively optically thin, or moderately optically thick at most. The observed lines of HCO^+ are only included at positions away from $\Delta\alpha = 20''$, because the $3 \rightarrow 2$ and $4 \rightarrow 3$ lines are probably more optically thick at the peak position. The HCN lines are not used since the presence of hyperfine components in the $3 \rightarrow 2$ line at velocity separations of $1-2$ km s^{-1} broadens the lines, effectively reducing the difference between the two components in terms of line width and thus prohibiting a reliable determination of their relative contributions given the signal to noise ratio of the data. The observed transitions for the included species are sensitive to a wide range of excitation regimes, covering densities up to a few$\times 10^7$ cm^{-3} and temperatures up to 200 K.

Since in the optically thin limit the intensity scales linearly with the molecular column density, the intensity ratio of two transitions of the same molecule is independent of column density and depends only on the density and temperature. In Table 3 the observed ratios are listed. The relative errors are estimated at about 60%. At $\Delta\alpha = 20''$, the signal–to–noise is at its best, and confusion with the second velocity component is minimal, so that the error at this position is no larger than about 30%. Ratios derived from transitions which were observed more than once, either with the same telescope or with different telescopes, agree to within this level.

It can be seen from Table 3 that for most combinations of observed transitions no significant variations are found at the different positions across the Bar *within the estimated errors*. For a number of observed ratios, substantial deviations are found, which are marked in the table. With the exception of $C^{18}O$, these deviations show no large, systematic behavior, and can usually be attributed to uncertainties in the fit parameters of one of the observed lines. The important implication of this finding is that the physical properties of the gas traced by these species do not change largely across the Bar.

In order to constrain the physical parameters, first a homogeneous model with a constant temperature and density was constructed. To this end, the statistical equilibrium populations of the levels were computed for a given H_2 number density, kinetic temperature, and molecular column density. Instead of a specified cloud geometry, the calculation assumes an escape probability for the photons, which depends on the ratio of the column density of the molecule and the line width ΔV (1.8 km s^{-1} in our case) (see Jansen et al. 1994a for details). The details of the radiative transfer are not essential since most lines considered here will turn out to be optically thin. The intensity of any background radiation field also has to be specified. We have included the 2.73 K cosmic background radiation, which is the most important part of the overall (galactic) background at millimeter wavelengths. Radiative excitation by the warm dust does not affect the results for the rotational transitions of the heavy rotors considered here. Only collisions with H_2 were considered. Collisions with electrons start to be significant for electron fractions $x_e = n_e/n_{H_2} > 10^{-5}$. In PDR's, the electron density is about equal to the abundance of C^+, the major donor of electrons when hydrogen is neutral. At the Orion Bar, the [C II] observations of Boreiko et al. (1988), as well as unpublished data by Keene & van Dishoeck (1991) give $N(C^+) \simeq 2\,10^{18}$ cm^{-2}, corresponding to $x_e \sim 5\,10^{-5}$ for an H_2 column density of $\sim 5\,10^{22}$ cm^{-2}

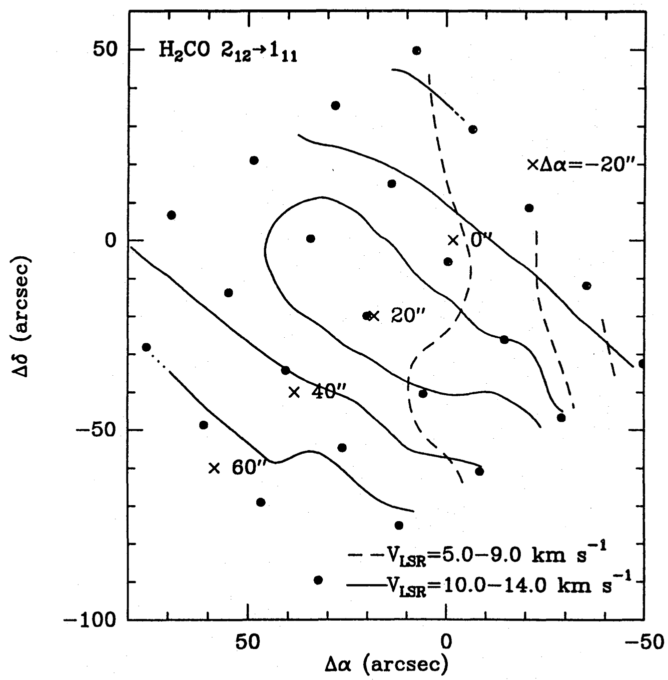

Fig. 4. Integrated intensity of H_2CO $2_{12} \rightarrow 1_{11}$ toward the Orion Bar. Drawn contours correspond to the velocity component associated with the Bar (integration interval 10.0 – 14.0 km s^{-1}), dashed contours correspond to a foreground or background cloud (integration interval 5.0 – 9.0 km s^{-1}). Contour levels start at 10 K km s^{-1} and increase in steps of 5 K km s^{-1}, in units of T_R^*. Data have been obtained with the NRAO 12m telescope (beam size 45″) at the positions of the dots. The crosses indicate the five observed positions

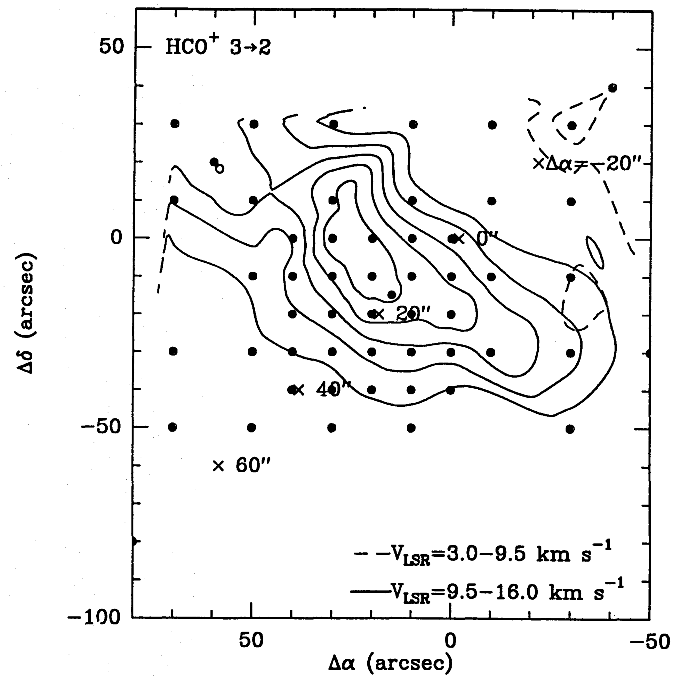

Fig. 5. Integrated intensity of HCO^+ 3 $\rightarrow$ 2 toward the Orion Bar. Drawn contours correspond to the velocity component associated with the Bar (integration interval 9.5 – 16.0 km s^{-1}), dashed contours correspond to a foreground or background cloud (integration interval 3.0 – 9.5 km s^{-1}). Contour levels start at 10 K km s^{-1} and increase in steps of 5 K km s^{-1}, in units of T_A^*. Data have been obtained with the JCMT (beam size 21″) at the positions of the dots. The crosses indicate the five observed positions

(see Sect. 5.2). Also, Tielens & Hollenbach (1985b) estimate that the electron density is $\sim$ 60 cm^{-3} from the required photoelectric heating efficiency needed to produce the observed kinetic temperature inferred from the [O I] 63 μm observations. This electron density may correspond to an electron abundance as high as 10^{-4}, but refers to the region were the bulk of the [C II] 158 μm, [O I] 63 μm and thermal infrared emission is coming from. The region sampled here lies at a somewhat larger A_V, where most carbon is in the form of CO, and thus has a lower electron density. For example, Fig. 6 of Tauber et al. (1994) shows that at this stage the electron density is less than 10^{-6}. This justifies the omission of electrons as collision partners. To study the relative excitation of the lines, model calculations were performed using a molecular column density of 10^{12} cm^{-2}, low enough to ensure optically thin excitation.

Figures 8 and 9 compare the observed peak line intensity ratios for CS, $C^{18}O$, HCO^+ and H_2CO at all positions with the outcome of the model calculations. In Table 3 the derived densities are listed. The kinetic temperature is constrained from two sets of observations. First, the observed intensity of the optically thick ^{12}CO 3→2 line provides an estimate of the temperature $T_{kin} \approx 100$ K across the Bar, assuming no further beam dilution. Second, the H_2CO $3_{22} \rightarrow 2_{21}/3_{03} \rightarrow 2_{02}$ line ratio is mainly sensitive to temperature for densities larger than $\sim 5\,10^3$ cm^{-3} (van Dishoeck et al. 1993; Mangum & Wootten 1993). The observed ratios indicate $T_{kin} \approx 85 \pm 30$ K, with no significant variation across the Bar (see Fig. 9). The other observed ratios are mainly sensitive to density, and much less to the kinetic temperature. No single density is found to fit all the data. Instead, a range of densities between $\sim 10^4$ cm^{-3} and $\sim 10^7$ cm^{-3} is inferred, depending on the critical density of the transitions involved. The CS 3 $\rightarrow$ 2/2 $\rightarrow$ 1 ratio, for example, probes lower densities than the CS 7 $\rightarrow$ 6/5 $\rightarrow$ 4 ratio (see Fig. 8b). The observed H_2CO $7_{17} - 6_{16}/5_{15} - 4_{14}$ ratio indicates densities of at most 10^7 cm^{-3} at $\Delta\alpha$ = 15″. No significant variations larger than a factor of 3 in density are inferred across the Bar. The only exception is formed by the transitions of $C^{18}O$, which trace a much lower density at positions away from the emission peak (Fig. 8a). At the peak position, these lines are thermalized, and indicate a kinetic temperature of $\sim$ 90 K, consistent with the ^{12}CO and H_2CO results.

5. Inhomogeneous models

5.1. Two–component model

In Sect. 4 it was found that a single density model cannot explain the observed line ratios, but that a range of densities appears present within the beam. Whether different temperatures are involved as well is not clear. As a first order approximation, we have constructed a model with two density components at

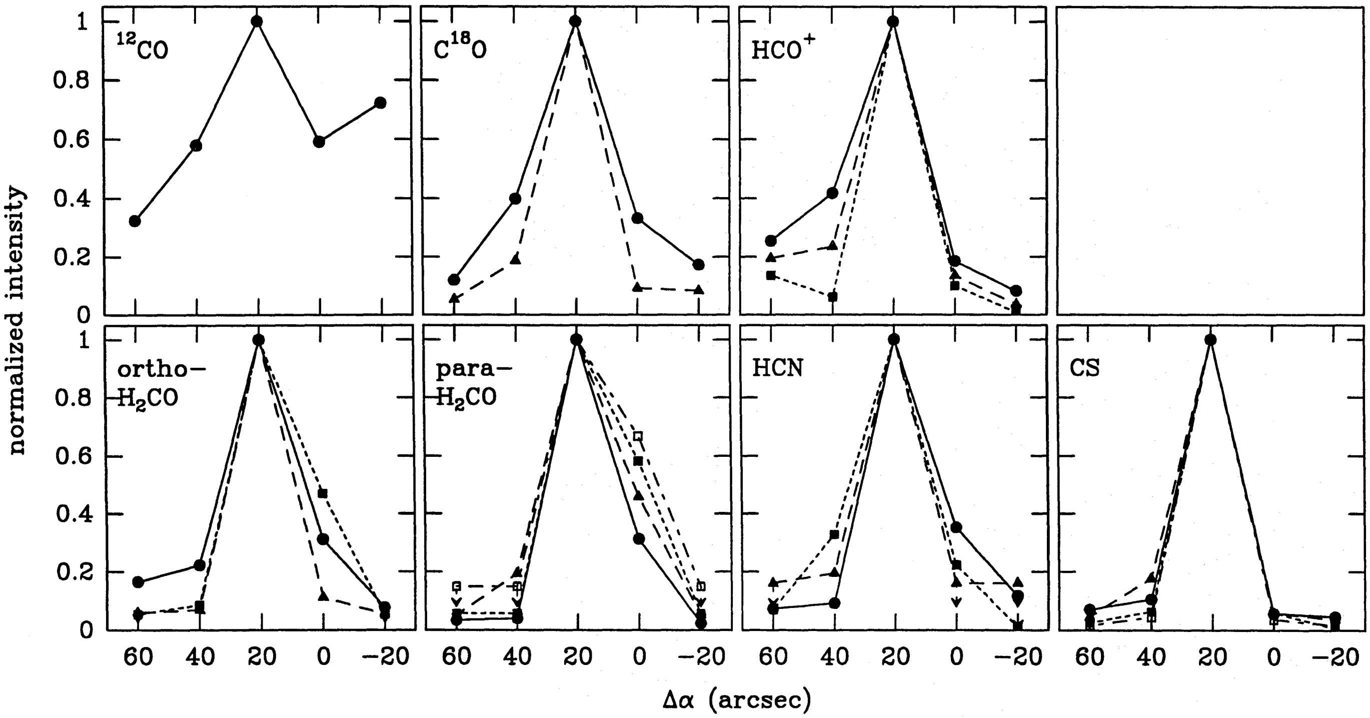

Fig. 6. Normalized intensity distribution of observed lines toward the Orion Bar. The Trapezium stars are to the right side of each plot. Horizontal scale is $\Delta\alpha$ in arcsec, vertical scale is antenna temperature normalized with respect to the peak value at $\Delta\alpha = 20''$. The meaning of the symbols is as follows: ^{12}CO 3 → 2 dots; C^{18}O 2 → 1 dots, 3 → 2 triangles; HCO$^+$ 1 → 0 dots, 3 → 2 triangles, 4 → 3 filled squares; ortho–H_2CO $2_{12} \rightarrow 1_{11}$ dots,$3_{12} \rightarrow 2_{11}$ triangles, $5_{15} \rightarrow 4_{14}$ filled squares; para–H_2CO $3_{03} \rightarrow 2_{02}$ dots, $3_{22} \rightarrow 2_{21}$ triangles, $3_{21} \rightarrow 2_{20}$ filled squares, $5_{05} \rightarrow 4_{04}$ open squares; HCN 1 → 0 dots, 3 → 2 triangles, 4 → 3 filled squares; CS 2 → 1 dots, 3 → 2 triangles, 5 → 4 filled squares, 7 → 6 open squares

a constant temperature. Because of the insensitivity of most ratios to temperature, the assumption of constant temperature will have no great effect on the conclusions. In this two–component model a certain fraction of the molecular column density is comprised in high–density regions, while the remaining part resides in low–density regions. Instead of explicitly assuming a beam filling factor of the high density material, the fraction of molecular column density in the clumps is varied. Although no assumptions are made on the spatial distribution of the two components other than that they are both present in our telescope beam, we will use the picture of high density clumps embedded in a low density interclump medium, similar to Burton et al. (1990) and Tauber et al. (1994). The excitation of each component has been calculated separately using the same excitation code as described above. The temperature is taken to be 85 K and the line width 1.8 km s^{-1} for both density components. The peak line intensities of the two components are subsequently added to obtain the total emission for comparison with observations. In this procedure, it is implicitly assumed that optical depth effects do not play any role. The models were made for the ratios of the observed transitions of CS, C^{18}O, HCO$^+$ and H_2CO, for clump– and interclump densities ranging from 10^3 cm^{-3} to 10^8 cm^{-3}, and assuming 10%, 30% or 50% of the total column density in the clumps.

To obtain a quantitative comparison between models and observations, the following parameter has been constructed:

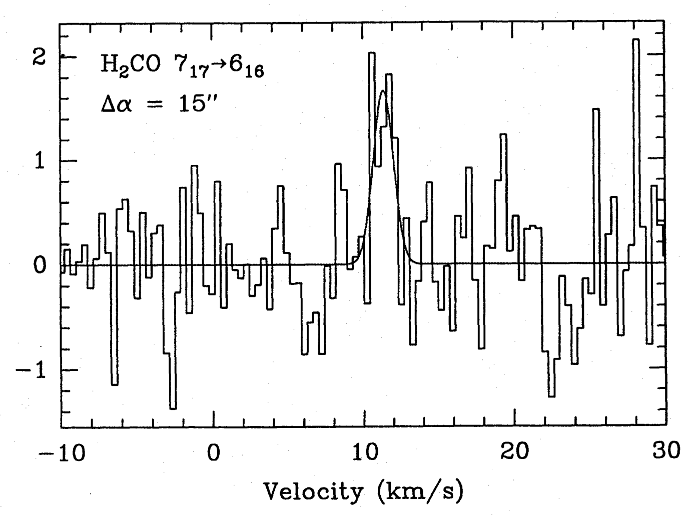

Fig. 7. 2σ detection of H_2CO $7_{17} \rightarrow 6_{16}$ toward $\Delta\alpha = 15''$ obtained with the JCMT. Horizontal scale is $V_{\rm LSR}$ in km s^{-1}, vertical scale is antenna temperature $T_{\rm R}$ in K

$$\chi^2 = \frac{1}{M} \sum \left(\frac{\text{ratio(model)} - \text{ratio(obs)}}{\Delta(\text{obs})} \right)^2 , \qquad (1)$$

where summation is over all ratios at $\Delta\alpha = 20''$ of observed transitions, M in total, and Δ(obs) is the estimated absolute error in the observed value. The best fit to the data is obtained for the

Table 4. Best fit parameters for the Orion Bar molecular gas

clump–n_{H_2}	$1^{+3.0}_{-0.7}\ 10^6\ \mathrm{cm}^{-3}$
interclump–n_{H_2}	$3^{+2.0}_{-2.2}\ 10^4\ \mathrm{cm}^{-3}$
clump volume filling factor	$\sim 0.3\%$
kinetic temperature T_{kin}	85 ± 30 K

set of parameters which minimizes χ^2. Since the model should not deviate from the observations by more than the average error, only models with $\chi^2 \lesssim 1$ are acceptable. In Fig. 10, contour plots of χ^2 as functions of clump and interclump density are presented for the three fractions of total molecular material in the clumps. Note that since the density ranges of the clump and the interclump gas in the model are equal, points on the diagonal line in each diagram correspond to homogeneous models, while points in the upper left corner of each diagram correspond to 'swiss–cheese' rather than 'clump–interclump' models.

From these plots it is seen that inhomogeneous models give a somewhat better fit to the data, but that the difference with homogeneous models (on the diagonal line) is not large. The χ^2 criterion constructed here depends on the excitation properties of the included transitions, and since most of the observed lines have comparable excitation properties, the χ^2 is only moderately sensitive to different densities. Because not many high excitation lines have been taken into account, the results are biased toward lower densities. Nevertheless, a firm conclusion is that the interclump density cannot be larger than $10^5\ \mathrm{cm}^{-3}$. Furthermore, it is seen that the best fit models (with $\chi^2 \lesssim 1$) are limited to a relatively small region in parameter space: 10% of the total material in the clumps, $3\ 10^5$ <clump–n_{H_2}< $4\ 10^6\ \mathrm{cm}^{-3}$ and $8\ 10^3$ <n_{H_2}< $5\ 10^4\ \mathrm{cm}^{-3}$ for the interclump gas. The best fit value, indicated by the filled triangle in Fig. 10, is $\chi^2 \sim 1.0$ for clump–n_{H_2}= $10^6\ \mathrm{cm}^{-3}$, interclump–n_{H_2}= $3\ 10^4\ \mathrm{cm}^{-3}$.

Tauber et al. (1994) and Tielens et al. (1993) derive an interclump density for the Bar from the spatial separation of the peaks of the PAH emission, the vibrational H_2 emission and the ^{12}CO 1 $\rightarrow$ 0 emission. They find that an interclump density of $\sim 5\ 10^4\ \mathrm{cm}^{-3}$ is able to provide the required attenuation of the far–ultraviolet field on the observed scales. This value is an upper limit, since a small inclination of the PDR would increase the spatial separation corresponding to the observed angular separation. About the same value for the interclump density is found from the derived H_2 column density (from ^{13}CO 1 $\rightarrow$ 0) and the inferred length of the line–of–sight (0.12 pc), needed to account for the observed infrared flux of dust of $\sim$ 75 K (Werner et al. 1976). Both values are in excellent agreement with our findings.

In summary our observations are best described by a clump–interclump model with a clump volume filling factor of 0.3%, a clump density of $(0.3 - 4.0)\ 10^6\ \mathrm{cm}^{-3}$, an interclump density of $(0.8 - 5.0)\ 10^4\ \mathrm{cm}^{-3}$ and a kinetic temperature for both components of 85 ± 30 K (see Table 4). No significant variation in these parameters is found across the Bar. The large uncertainty introduced by the quality of the data, the presence of the second velocity component and the sensitivity to e.g. small pointing errors does not permit any refinement of this two component model.

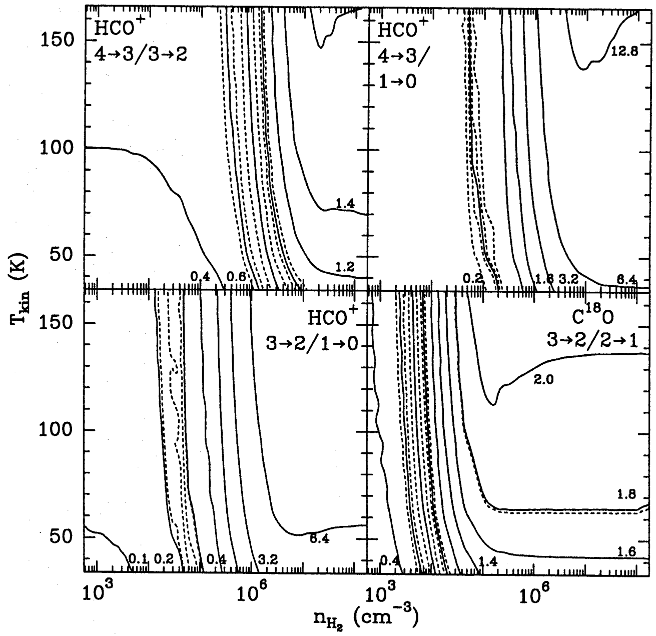

Fig. 8a. Peak line intensity ratios of HCO^+ and $C^{18}O$ as functions of H_2 number density and kinetic temperature in a homogeneous density model. Dashed regions indicate observed values at $\Delta\alpha = 20''$ or average observed values across the Bar

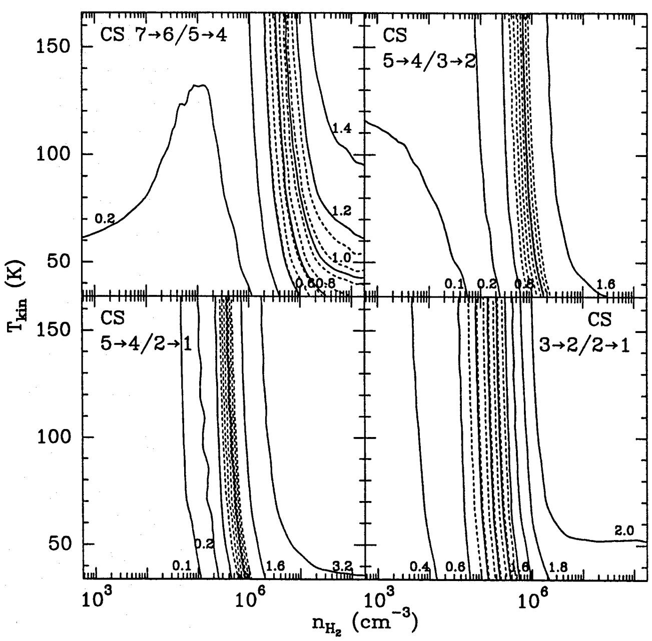

Fig. 8b. Peak line intensity ratios of CS as functions of H_2 number density and kinetic temperature in a homogeneous density model. Dashed regions indicate observed values at $\Delta\alpha = 20''$ or average observed values across the Bar

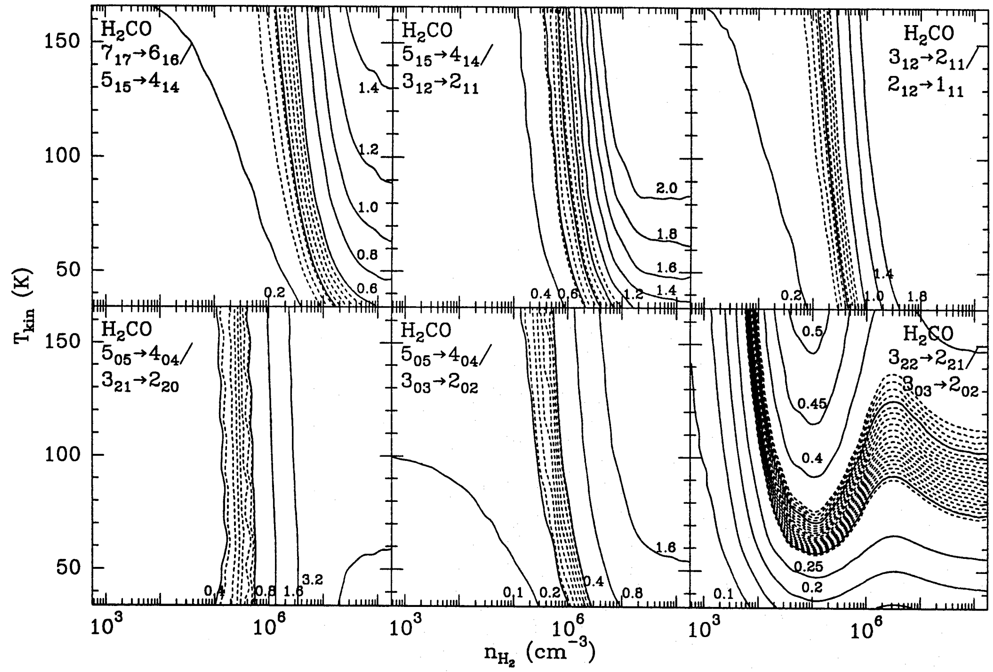

Fig. 9. Peak line intensity ratios of H_2CO as functions of H_2 number density and kinetic temperature in a homogeneous density model. Dashed regions indicate observed values at $\Delta\alpha = 20''$ for ortho– and para–H_2CO line ratios. The observed $7_{17} \rightarrow 6_{16}/5_{15} \rightarrow 4_{14}$ ratio should be regarded as an upper limit

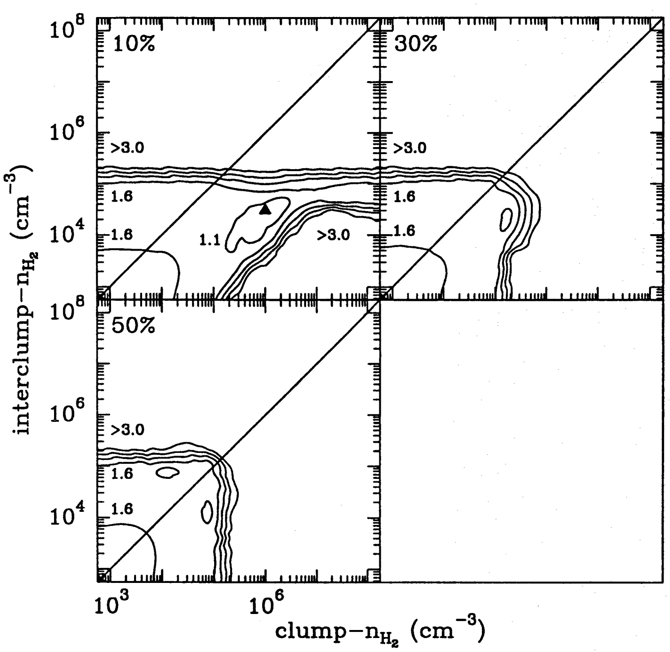

Fig. 10. χ^2 of observed and modelled intensity ratios, as defined in the text, for 10%, 30% and 50% of total molecular material in the clumps. The diagonal lines correspond to homogeneous density models, the upper left corners to 'swiss-cheese' models. The clump and interclump density are constrained to (0.3 – 4.0) 10^6 and (0.8 – 5.0) 10^4 cm^{-3}, respectively, with best fit value $\chi^2 \approx 1$ for clump–n_{H_2}= 1.0 10^6 and interclump–n_{H_2}= 3.0 10^4 cm^{-3} (indicated by filled triangle). A kinetic temperature of 85 K has been assumed for both components

5.2. Determination of molecular column densities

The same two–component model described above has been used to constrain the molecular column densities of the various species. Whereas the density and the temperature have been derived from line intensity ratios, the molecular column densities are determined from the absolute intensities. Since the adopted code provides also estimates of the opacity, the approximation that the lines are optically thin could be checked, and proved valid at positions away from the emission peak ($\Delta\alpha \neq 20''$). Since no significant variations in density or temperature were found across the Bar (see Sect. 5.1), the observed emission peak must correspond to a peak in molecular column density. At the peak position, it was found that the interclump gas has optical depths of order unity or larger for some species (see Sects. 3 and 4). Because of the low density of the interclump gas however, most levels involved are subthermally populated. Absorption of a photon therefore leads to radiative rather than collisional de–excitation, returning the photon to the radiation field, so that the line emission is moderately attenuated at most. This validates the assumption of optically thin excitation in the determination of the physical parameters (Sect. 5.1).

In the determination of the molecular column densities a first order correction was made for the opacity of the interclump gas by attenuating the emission of the clumps by the corresponding column of interclump gas. The resulting antenna temperatures at $\Delta\alpha = 20''$ are presented in Table 5 and are compared with observations. Note that this is the first time that the assumption that the high and low density phases are spatially coexistent is used. For ^{12}CO a kinetic temperature of 120 K was used to fit the observed value of the 3 → 2 line. Except for HCN 4 → 3, the model intensities are similar to the observed intensities to within 30% (the expected error level). In particular, the observed lines of $C^{34}S$ and $H^{13}CO^+$ are consistent with model predictions for abundance ratios of 1/22 and 1/67 respectively. The molecular abundances in the clumps are not necessarily the same as in the interclump gas. In particular, the abundance of the ion HCO^+ is

Table 5. Contributions to the line emission from the high and low density phases at $\Delta\alpha = 20''$ [a]

Molecule	Transition	$N_{\rm mol}$ $\rm cm^{-2}$	$T_{\rm R}$ (K) interclump	$T_{\rm R}$ (K) clump	$T_{\rm R}$ (K) total*	$T_{\rm R}$ (K) observed
CS	$2 \rightarrow 1$	$1.5\,10^{15}$	15.4	11.0	18.0*	17.9
	$3 \rightarrow 2$		13.3	17.4	21.3*	19.1[b]
	$5 \rightarrow 4$		5.8	15.4	17.6*	14.0
	$7 \rightarrow 6$		1.5	7.5	9.0	9.4[b]
	$10 \rightarrow 9$		0.1	0.9	1.0	
$C^{34}S$	$5 \rightarrow 4$	$6.8\,10^{13}$	0.3	1.1	1.4	1.2
HCN	$1 \rightarrow 0$	$3.0\,10^{14}$	7.2	8.9	10.7*	11.2
	$3 \rightarrow 2$		2.4	7.5	9.2*	12.1[b]
	$4 \rightarrow 3$		1.0	4.2	5.1*	11.9[b]
HCO^+	$1 \rightarrow 0$	$2.0\,10^{14}$	21.0	5.1	22.0*	27.5
	$3 \rightarrow 2$		10.1	18.3	22.3*	16.5[b]
	$4 \rightarrow 3$		5.7	15.2	18.3*	19.7[b]
$H^{13}CO^+$	$3 \rightarrow 2$	$3.0\,10^{12}$	0.3	0.4	0.7	0.7
ortho–H_2CO	$2_{12} \rightarrow 1_{11}$	$3.0\,10^{14}$	6.8	2.6	7.5*	7.1
	$3_{12} \rightarrow 2_{11}$		2.5	3.9	5.5*	4.4
	$5_{15} \rightarrow 4_{14}$		1.1	3.2	4.3	3.7
	$7_{17} \rightarrow 6_{16}$		0.2	0.9	1.1	1.5
	$5_{33} \rightarrow 4_{32}$		0.2	0.6	0.8	
para–H_2CO	$3_{03} \rightarrow 2_{02}$	$1.0\,10^{14}$	1.6	2.0	3.0*	3.2
	$3_{22} \rightarrow 2_{21}$		0.7	0.6	1.3*	1.2
	$5_{05} \rightarrow 4_{04}$		0.2	0.9	1.1*	0.9
	$7_{07} \rightarrow 6_{06}$		0.0	0.2	0.2	
	$5_{24} \rightarrow 4_{23}$		0.1	0.6	0.7	
HNC	$1 \rightarrow 0$	$6.0\,10^{13}$	2.7	2.4	4.2*	5.5
	$4 \rightarrow 3$		0.2	0.9	1.1	1.1
$C^{18}O$	$2 \rightarrow 1$	$1.3\,10^{16}$	7.7	0.5	8.2	8.5
	$3 \rightarrow 2$		13.1	1.0	14.0	15.3
^{13}CO [c]	$1 \rightarrow 0$	$9.8\,10^{16}$	14.0	1.1	15.1	
	$2 \rightarrow 1$		40.9	3.8	44.7	
	$3 \rightarrow 2$		54.6	7.4	56.2*	
	$4 \rightarrow 3$		52.6	10.6	54.7*	
	$6 \rightarrow 5$		36.6	13.6	41.4*	
	$7 \rightarrow 6$		24.2	12.9	31.6*	
^{12}CO [c]	$1 \rightarrow 0$	$6.5\,10^{18}$	114.1	49.0	114.1*	
	$2 \rightarrow 1$		112.0	99.2	112.0*	
	$3 \rightarrow 2$		109.4	109.4	107.8*	109.4
	$4 \rightarrow 3$		106.6	108.3	108.3*	
	$6 \rightarrow 5$		100.2	103.1	103.1*	
	$7 \rightarrow 6$		96.7	100.3	100.3*	90.0[d]
	$14 \rightarrow 13$		16.2	8.1	24.3	14.0[d]

* Marked values include a correction for the opacity of the interclump gas.
[a] Clump–$n_{\rm H_2}$ = $1\,10^6$ $\rm cm^{-3}$, interclump–$n_{\rm H_2}$ = $3\,10^4$ $\rm cm^{-3}$, 10% of total material in the clumps.
[b] Peak temperature derived from integrated antenna temperature assuming ΔV = 1.8 $\rm km\,s^{-1}$.
[c] Using $T_{\rm kin}$=120 K for ^{12}CO and ^{13}CO.
[d] From Stacey et al. (1993).

expected to be decreased in the clumps. In general, all derived column densities are sensitive to the density in the interclump gas: if this were as high as 10^5 $\rm cm^{-3}$, all column densities would be lower by a factor of 3. Predictions for the strengths of higher excitation lines like CS $10 \rightarrow 9$, and for transitions of ^{13}CO, using $T_{\rm kin}$ = 120 K, can be found in Table 5 and Fig. 11.

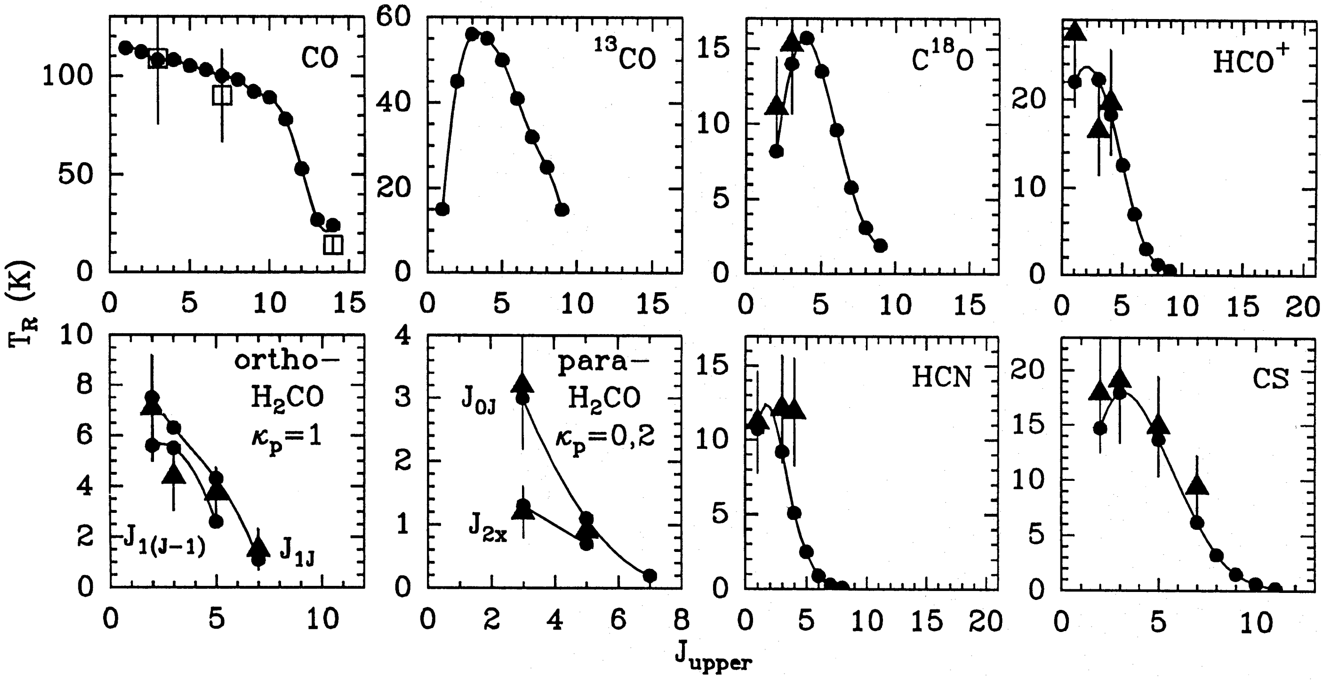

Fig. 11. Peak line intensities at $\Delta\alpha = 20''$ predicted by the proposed model for the Orion Bar PDR as functions of the J–value of the upper level. Observations are indicated by triangles (our observations) and open squares (^{12}CO Stacey et al. 1993). For ortho–H$_2$CO only the $\kappa_p = 1$ ladder has been plotted, with the top line referring to $2_{12} \rightarrow 1_{11}$ etc., and the lower line to $2_{11} \rightarrow 1_{10}$ etc.; for para-H$_2$CO only $3_{03} \rightarrow 2_{02}$, $5_{05} \rightarrow 4_{04}$, $7_{07} \rightarrow 6_{06}$ (top line), and $3_{22} \rightarrow 2_{21}$, $5_{24} \rightarrow 4_{23}$ (lower line)

It was noted in Sect. 4 that the C^{18}O line ratio shows a significant and systematic variation across the Bar, tracing lower densities away from the emission peak. It is known that the Orion Bar lies in front of the cold Orion Molecular Cloud (OMC–1). Dutrey et al. (1993) present C^{18}O $1 \rightarrow 0$ and $2 \rightarrow 1$ observations of the region, and derive a C^{18}O column density of $\sim 1\,10^{15}$ cm^{-2}, an H$_2$ number density of $\sim 5\,10^3$ cm^{-3} and a kinetic temperature of $\sim$ 18 K, with most gas emitting at velocities around 10 km s^{-1}. This gas has a spatial distribution much larger than that of the Orion Bar. Because of the much lower spatial resolution of their observations (2$'$.5), the Bar itself is barely visible in their maps. The contribution of the OMC–1 to the observed C^{18}O intensities away from the emission peak is 50–70% for C^{18}O $2 \rightarrow 1$ and 15–25% for C^{18}O $3 \rightarrow 2$, and it is less than 10% for both lines at the emission peak. The relatively large contribution of the OMC–1 to the total observed intensity of the $2 \rightarrow 1$ line at $\Delta\alpha \neq 20''$ can explain the variation in line ratio across the Bar, and hence the variation in inferred density. Because of the low density and temperature, the only contribution of the OMC–1 to our observed lines is expected in C^{18}O. For example, no detection of H$_2$CO $2_{12} \rightarrow 1_{11}$ was made at $\Delta\alpha > 80''$ at a noise level of 0.15 K in observations made with the NRAO 12m. From the background OMC no more than $T_R \approx 0.1$ K is expected for this line, assuming an H$_2$CO column density of $\sim 4\,10^{12}$ cm^{-2}, i.e. the same H$_2$CO/C^{18}O ratio as in the Bar, and the same physical parameters as for C^{18}O. This gas is therefore distinct from the second velocity component found in our data at $V_{LSR} \approx 9$ km s^{-1}, which is seen in H$_2$CO. It is concluded that the background OMC can explain the inferred density variation across the Bar as traced in C^{18}O, but that the inferred column density is only marginally affected for $2 \rightarrow 1$ and not significantly for $3 \rightarrow 2$. It is also concluded that the known presence of the OMC–1 behind the Orion Bar PDR makes any model based on CO which does not include the OMC–1 incomplete.

The C^{18}O column densities of the Bar have been used to derive H$_2$ column densities using an H$_2$/C^{18}O ratio of $10^4 \times 500 = 5\,10^6$ (i.e. H$_2$/^{12}CO $\times$ ^{12}CO/C^{18}O). This H$_2$/C^{18}O ratio is somewhat larger than the value of $3\,10^3$ found by Lacy et al. (1994) in the neighboring NGC 2024 region, but reflects the fact that not all carbon is in CO in this PDR. Also, C^{18}O may be still selectively photodissociated in this regime of column densities (van Dishoeck & Black 1988). The inferred H$_2$ column densities are subsequently used to determine the fractional molecular abundances (see Paper II) and to estimate the length of the line–of–sight through the Orion Bar, since the H$_2$ densities are known. Both the H$_2$ column densities and the corresponding lengths are listed in Table 6.

5.3. Alternative clump models

In the previous section we have seen that the intensities of the observed transitions are best fit by a model where the material is distributed inhomogeneously. We have performed a very crude modeling of the radiative transport in such a clumpy medium, which only gives accurate results in the optically thin limit. In this section we will investigate other methods that have been

Table 6. H_2 column density and length of line–of–sight

$\Delta\alpha$	N_{H_2} [a]	ℓ [b]	
″	cm^{-2}	cm	pc
−20	6.5 10^{21}	2.2 10^{17}	7.2 10^{-2}
0	6.5 10^{21}	2.2 10^{17}	57.2 10^{-2}
20	6.5 10^{22}	2.2 10^{18}	71.5 10^{-2}
40	2.0 10^{22}	6.5 10^{17}	21.1 10^{-2}
60	4.6 10^{21}	1.6 10^{17}	5.1 10^{-2}

[a] Derived from $C^{18}O$ 3 → 2 assuming $H_2/C^{18}O = 5\,10^6$.
[b] Length of line–of–sight estimated by dividing H_2 column density by volume density of interclump gas.

used in the literature to analyze and model the emission from a clumpy medium, especially that of CO.

5.3.1. Radiative transport in a clumpy medium

Martin et al. (1984) present a simple model for the emission from an isothermal cloud composed of randomly moving fragments (clumps) which are in local thermodynamic equilibrium (LTE). Genzel et al. (1990) have extended their model to include non–LTE excitation. The main result of these models is that the observed profiles seem less saturated than those according to models of microturbulent clouds with the same column density. This can be explained by the fact that clumpy clouds can 'hide' material in optically thick clumps at velocities away from the line center. In the limit that both the clumps and the cloud as a whole are optically thin, the results of this modeling are equivalent to the results of a microturbulent model. This is an obvious result: the distribution of matter is of no importance to a photon which can escape the cloud unhampered. Since this is the case for most lines in the Orion Bar, we conclude that our rough treatment of the radiative transport in this clumpy cloud is sufficient.

5.3.2. Implications for clumpiness from the observed line profiles

In the above analysis no assumptions were made for the distribution of the two density components, other than that they are both present in the beam. Only to explain certain profiles both components need to be spatially coexistent. In an attempt to obtain information about the actual distribution, Tauber et al. (1991) investigated the autocorrelation function of ^{12}CO and ^{13}CO 1 → 0 line profiles obtained toward four positions in Orion A. The smoothness of the profiles, which are assumed to consist of the superposition of many narrow profiles of individual clumps, is determined by the presence or absence of a clump at a certain velocity following a Poisson distribution. Since for the Orion Bar even the highest excitation lines are influenced by the emission from the interclump gas, no conclusions can be drawn from their profiles on the distribution of the clumps. The autocorrelation functions of ^{12}CO 3 → 2 at $\Delta\alpha = -20''$

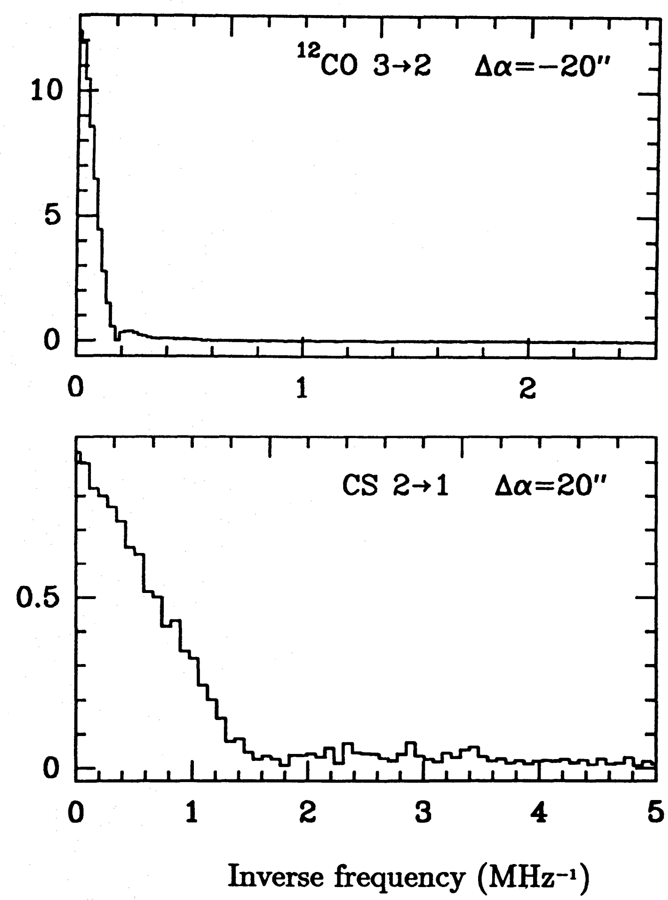

Fig. 12. Autocorrelation functions of the observed spectra of ^{12}CO 3 → 2 at $\Delta\alpha = -20''$ (top) and CS 2 → 1 at $\Delta\alpha = +20''$ (bottom). The horizontal scale is inverse frequency in MHz^{-1}, the vertical scale is intensity squared, in arbitrary units. The bump in the ^{12}CO autocorrelation function at ∼ 0.23 MHz^{-1} (∼ 3.8 km s^{-1}), and the tail of excess power (as compared to a Gaussian distribution) in the CS autocorrelation function, are indicative of the presence of two velocity components in the spectra

and CS 2 → 1 at $\Delta\alpha = 20''$ are shown in Fig. 12. The asymmetry of the line profiles is reflected in the presence of excess power with respect to a Gaussian distribution in their autocorrelation functions. Most notably, the autocorrelation function of ^{12}CO 3 → 2 shows a clear bump at an inverse frequency of 0.23 MHz^{-1}, corresponding to the a velocity correlation length of 3.8 km s^{-1} and related to the strong presence of the second velocity component at this position. The noise level does not permit the identification of any other velocity structure. Observations of the ^{12}CO 3 → 2 line made with 30″ (CSO) and 20″ (JCMT) beam sizes respectively show markedly distinct line profiles, indicating the presence of structure in the interclump gas on these scales.

6. A physical model for the Orion Bar

In the previous section we have seen that the gas traced by the observed molecular transitions shows no variation in temper-

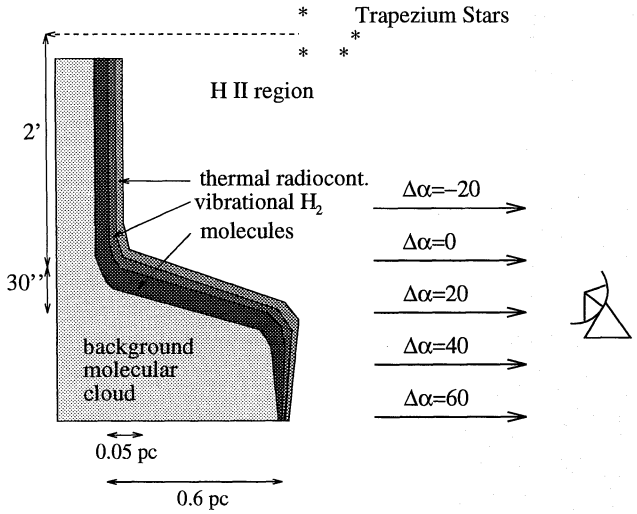

Fig. 13. Schematic view of the proposed geometric model for the Orion Bar. The emission peak is caused by the increased length of the line–of–sight as the PDR changes from a face–on to an edge–on orientation

ature or density across the Bar. The only exception is $C^{18}O$, for which the variation can be attributed to the presence of the low density, cold Orion Molecular Cloud. We have derived a model where the gas is distributed in dense clumps dispersed in a lower density interclump medium with low volume filling factor. Within this model, the observed emission peak corresponds to a peak in molecular column density. All molecules show the same spatial distribution and no variations in molecular abundances are found (Paper II). The only explanation for such a behavior is a geometric one.

6.1. A purely geometrical model

If the variation in H_2 column density derived from the $C^{18}O$ observations is interpreted as a variation in the length of the line–of–sight through the gas, the following geometric model can be constructed. At the extreme positions ($\Delta\alpha = -20''$ and $60''$), the PDR is viewed face–on. From $\Delta\alpha = -20''$ to $\Delta\alpha = 60''$, the PDR changes from a face–on to an edge–on geometry, and back to a face–on geometry. A schematic view of this model is presented in Fig. 13. The sharp peak in the line–of–sight by a factor of 10 corresponds to the PDR having an edge–on geometry over a length of 10 times its typical thickness. The thickness of the PDR is found from the $C^{18}O$ column density at $\Delta\alpha = -20'', 60''$ to be 0.08 to 0.05 pc (see Table 6).

This purely geometrical model can explain all our observations very well, as argued above. The remaining question is how this geometry could have originated. One possibility is that we are just looking at the irregular structure of the original cloud complex. Another possibility could be the following. It is known that the Trapezium stars lie to the front of the OMC from which they were formed. Their expanding H II region has created a cavity in the cloud, which bursts out of the cloud on the front side. This is the blister or champagne model (Icke et al. 1980; Tenorio–Tagle 1979). The interface of the cavity and the low density OMC has been compressed by the expansion to a density of $\sim 3\,10^4$ cm^{-3}, with small clumps of $\sim 1\,10^6$ cm^{-3} with a low volume filling factor. The ultraviolet radiation longward of the Lyman–limit has created a PDR in this clumpy interface layer. If this bowl–shaped cavity were slightly inclined with respect to the plane of the sky, the Orion Bar would be the place where our line–of–sight is along one side of this bowl. Because of the relatively large density of the interclump gas and the low filling factor of the clumps, the thickness of the PDR is determined by the interclump gas, and hence it shows the clear, layered structure as seen by Tielens et al. (1993) on scales of 15''. The extension of the PDR for $\Delta\alpha > 40''$ could be partially due to the presence of θ^2A Ori, which apparently affects the chemistry and ionization but not the structure of the cloud.

This model also accounts for the observations of other groups. In particular, it fits very well with the distribution of [C I] 609 μm as reported by Tauber et al. (1994). They find that the distribution of the [C I] line is symmetric around the peak of the molecular emission. This cannot be explained by the model they propose, which is simply a large clump illuminated from one side by the Trapezium stars. In that case, the [C I] has to peak slightly in front of the CO. In our model, a complete PDR is seen at every position, but with a varying length of the line–of–sight through it. This naturally explains the observed [C I] distribution.

Our model also agrees with the [C II] 158 μm map of the Orion region from Stacey et al. (1993). There the [C II] is seen to peak not only at the ionization front, but also to be distributed symmetrically around it. Although the spatial resolution is not very high, [C II] emission is clearly present 'behind' the Bar (with respect to the Trapezium stars). Such extended [C II] emission has often (and rightly) been seen as evidence of the clumpiness of a cloud. Although the Orion Bar is clumpy, the structure of its PDR is governed by the rather dense, homogeneous interclump gas, and the extended distribution of [C II] has a different, geometric origin.

The observations of H_2 $v = 1 \rightarrow 0$ S(1) and $v = 2 \rightarrow 1$ S(1) by Hayashi et al. (1985) do not agree with our model. The value for their ratio at $\Delta\alpha = 20''$ of about 3 is lower than the prediction of our model ($\sim$ 10 for densities of $\sim 10^6$ cm^{-3}, assuming that the H_2 emission is dominated by the clumps, Sternberg & Dalgarno 1989). Hayashi et al. also find a variation in the line ratio across the Bar, in contradiction with our model. Recent measurements of these transitions with better instrumentation show no variation, however, and give a ratio of about 10, fully consistent with our model (Oliva, private communication). From the quality of the spectra shown by Hayashi et al. it is doubtful whether their conclusions are justified. As a result, there is also no evidence any longer for a significant shock at the Orion Bar, consistent with the small line widths observed in this work and the lack of variations in molecular abundances.

The pure rotational H_2 lines observed by Parmar et al. (1991) give results in accord with our model. They have sampled the Bar at much smaller spatial scales, about 1'' steps, and can thus distinguish the variations within the part of the PDR seen edge–on. Their inferred column density of H_2 of $1.6\,10^{21}$ cm^{-2} is much lower than our peak value of $5.0\,10^{22}$ cm^{-2}. However, they only sample a thin layer of hot molecular gas (> 400 K), while our column density is derived from the $C^{18}O$ column density of the warm gas (∼ 85 K).

The ^{12}CO column density inferred by Graf et al. (1990) of ∼ $3\,10^{18}$ cm^{-2} for gas at temperatures of 70 K or more is very close to our column density of ∼ $6\,10^{18}$ cm^{-2}. Their observations refer to $\Delta\alpha = 0''$ however, while our value refers to $\Delta\alpha = 20''$. The similarity of the two results can be explained by the shape of their beam, which has a FWHM of 8″ with considerable power in a pedestal of 40″ FWHM. This means that they were also sensitive to the peak at $\Delta\alpha = 15''$. Their conclusion that current PDR models are unable to explain such large columns of warm molecular gas does not hold for the specific case of the Orion Bar, however. Most PDR models to date assume that the line–of–sight is coincident with the line traversed by the far–ultraviolet photons. In the Orion Bar, the line–of–sight is perpendicular to the path of the far–ultraviolet photons, so that much larger columns of warm gas can be found. From the modeling of the CO–chemistry and the radiative transfer in PDR's Köster et al. (1994) reach the similar conclusion that the observed mid–J ^{12}CO and ^{13}CO line intensities cannot be explained by a single PDR layer seen face–on.

6.2. A less geometric interpretation

An alternative explanation for the observed peak in derived column density at the Orion Bar involves an enhancement of the clump filling factor. Such an explanation has recently been put forward by Wang et al. (1993) for M17 SW, which they studied in various transitions of CS and $C^{34}S$. This source is also a PDR viewed edge–on. A peak in molecular emission is found to lie outside the ionization front just as in the case of the Orion Bar. From the excitation analysis they find that the molecular gas has the same density everywhere, and that the peak in emission corresponds to a peak in column density. They also find that the gas is not distributed homogeneously, but is comprised in clumps much smaller than the telescope beam. Thus far, this source looks similar to the Orion Bar, although the distance to it is much larger (∼ 2 kpc instead of 450 pc). However, Wang et al. attribute the increase in column density to an enhancement in volume filling factor of the clumps, and not to an increase in the length of the line–of–sight. They reject the latter because there are more of these ridges found in other regions the sky, which are not parallel to any ionization front.

If the [C II] 158 μm observations of M17 SW (Stutzki et al. 1988) are compared to the [C II] observations of the Orion Bar, it is seen that their distribution is different. Toward M17 SW the [C II] emission is strongly peaked just outside the molecular peak, with an extended tail of moderate intensity emission into the surrounding cloud. Toward the Orion Bar, the [C II] emission is symmetric around the molecular peak and has a broad distribution. The extent of the emission in M17 SW is attributed to ultraviolet radiation which can penetrate to great depth into the clumpy cloud. The extent is in fact so large that internal ultraviolet sources or an enhanced, external, interstellar ultraviolet field is necessary to account for it. This makes it impossible to explain the observed emission distribution toward M17 SW as a pure geometrical effect only (Stutzki et al. 1988).

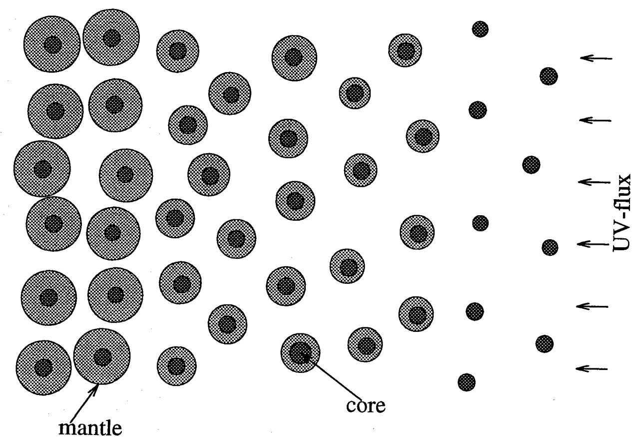

Fig. 14. Schematic picture of the Parmar et al. (1991) model for the Orion Bar. See text

On the other hand, the emission ridge/peak in M17 can still be explained by such a pure geometrical effect, especially considering the fact that molecular emission is detected at positions which lie in projection between the ionizing stars and the ionization front. The H II region in M17 could have created a cavity in the clumpy, surrounding cloud just as in our model for the Orion Bar. In fact, a less pronounced emission ridge is visible to the northeast as well. These ridges could be the edges of the cavity. Some ultraviolet radiation could penetrate to great depth into the cloud, accounting (partially) for the extended [C II] emission. Note, however, that the observed width of the emission ridge in M17 (30″) corresponds to 2′ at the distance of Orion A, i.e. of the same order as the Orion Ridge. This implies that the ridge in M17 SW is perhaps best compared to the Orion Ridge rather than to the Orion Bar. There is indeed no ionization front lying parallel to the Orion Ridge, but number and column density enhancements are found (e.g. Dutrey et al. 1993).

Inversely, we may ask whether the emission peak of the Orion Bar can be explained by an enhancement of clump filling factor instead of a geometrical effect. Any observed enhancement in column density derived from one or more transitions which trace the clumps can be attributed either to an increase in the length of the line–of–sight through the medium (geometrical interpretation) or to an increase in the number of clumps in a certain volume. Without any observations which trace the interclump gas, if there is any, no distinction between these two explanations can be made.

Most of the transitions observed here trace the interclump gas. Since these transitions show an emission peak, this lower density gas must have a column density peak at the Bar. Assuming that this gas is real interclump gas and is thus distributed homogeneously, the column density peak must correspond to a peak in the length of the line–of–sight. On the other hand, if our 'interclump' gas is interpreted as the mantles of larger clumps, and our 'clumps' as the dense cores of these large clumps, the emission peak could just as well correspond to a peak in the number of clumps per volume as to a peak in the line–of–sight length. There is no place for any interclump gas in this picture since this had to be visible in the transitions of low critical density. The 2 → 1 transition of $C^{18}O$ does trace low density gas, but this is necessarily very cold (~ 20 K) for otherwise it had to be visible in the 3 → 2 transition as well. Such a low temperature is unlikely for gas exposed to intense ultraviolet radiation, and the low density gas traced by $C^{18}O$ 2 → 1 most likely originates from the background OMC, which is shielded from the ultraviolet field of the Trapezium stars.

It is difficult, but not impossible, in the enhanced clump filling factor picture to explain the layered structure as shown by Tielens et al. (1993). One possible scenario is sketched by Parmar et al. (1991) (see Fig. 14). They propose that at the side of the cloud exposed to the ultraviolet radiation, the mantles are 'evaporated' leaving only the denser parts, and thus higher temperatures, giving rise to the H_2 emission. Deeper into the cloud, the mantles survive, and the temperature drops. As the mantles grow, shielding increases, and the inner parts of the cloud are only visible in molecular emission. This is in conflict with the extended distribution of [C II] emission, which requires less complete shielding. Also, different intensity distributions between high excitation and low excitation tracers should be visible. Such a difference is not found.

We conclude that a model which explains the observed emission peak at the Orion Bar by increasing the number density of clumps alone cannot account for the observed phenomena. In addition, no physical model has yet been brought forward for explaining the origin and stability of such regions of increased clump volume filling factor, although they may be observed elsewhere (Wang et al. 1993). Our model for the Orion Bar, which attributes the observed column density peak to a pure geometrical effect, as described in the previous section, has a natural explanation for its origin.

7. Summary

Observations of 53 transitions of 18 molecules, and isotopic varieties, at five positions on a strip crossing the Orion Bar PDR have lead to the following conclusions. The observed transitions show an emission peak of FWHM $\sim 30''$ at a position $\sim 30''$ (0.06 pc) outside the ionization front. On either side, the emission falls off to 10–20% of the peak value. All transitions show similar intensity distributions across the Bar.

An excitation analysis of the observed lines of CS, $C^{18}O$, H_2CO and HCO^+ has shown that no significant variations in H_2 number density or kinetic temperature exist across the Bar, within the uncertainties introduced by the signal–to–noise of the data, the presence of the second velocity component, and e.g. pointing errors. A limited contribution of the low temperature and density gas of the background Orion Molecular Cloud to the low excitation lines of $C^{18}O$ has been found. No single density model can describe the data satisfactory, and an inhomogeneous density distribution is constructed. A two component clump–interclump model is found to fit the data, using a kinetic temperature of 85 K. The best fit values of this model are: clump–$n_{H_2} \approx 1^{+3.0}_{-0.7}\,10^6$ cm^{-3}, interclump–$n_{H_2} \approx 3^{+2.0}_{-2.2}\,10^4$ cm^{-3} with ~10% of the total amount of molecular material comprised in the clumps.

Since no variations in density or temperature are found across the Bar, the observed emission peak corresponds to a molecular column density peak. A geometric interpretation for this column density peak is presented. Along the observed strip, the PDR is changing from a face–on to an edge–on orientation, and back. The emission peak is the location where the PDR is viewed edge–on over a length of about ten times its typical thickness (Fig. 13). This particular geometry can be interpreted within the champagne or blister model for the Orion H II region as the wall of the cavity blown out by the Trapezium stars.

Other observations (e.g. Tielens et al. 1993; Stacey et al. 1993; Parmar et al. 1991; Graf et al. 1990) are found to agree well with the presented model (see Sect. 6.1). Since our observations were obtained with relatively large beam sizes ($15'' - 30''$), only global properties of the PDR can be compared. Interferometric observations (e.g. Tauber et al. 1994) show the irregular, clumpy morphology that the Orion Bar exhibits on smaller scales. On larger scales, this irregularity is smoothed out. Observations with a spatial resolution of a few arcseconds are needed to probe the variations within the part of the PDR–layer seen edge–on.

The geometrical interpretation for the enhanced emission at the Orion Bar presented in this paper raises the question how common such geometrical effects are. On statistical grounds, geometry is unlikely to be the sole explanation for the widely observed [C I] 609 μm and [C II] 158 μm emission in other clouds. However, given the limited dynamic range of most maps, small geometrical effects may play a larger role than thought before. Such models will be particularly powerful for explaining the large columns of warm CO that have been observed in various clouds. PDR models in which the line–of–sight is not coincident with the path of the far–ultraviolet photons are currently being constructed (Spaans 1994). Specific results for the chemical modeling of the Orion Bar will be presented in a subsequent paper (Jansen et al. 1994b).

Acknowledgements. This work was supported by a PIONIER grant of the Netherlands Organization for Scientific Research (NWO). MRH is also grateful to the J.C. Kapteyn fund for travel support. F.P. Helmich, F. Baas and R.P. Tilanus are thanked for carrying out part of the observations. The referee J. Stutzki provided valuable comments on the manuscript.

References

Boreiko, R.T., Betz, A.L., Zmuidzinas, J., 1988, ApJ 325, L47
Burton, M.G., Hollenbach, D., Tielens, A.G.G.M., 1990, ApJ 365, 620
Dutrey, A., Duvert, G., Castets, A., et al., 1993, A&A 270, 468
Genzel, R., Stacey, G.J., Harris, A.I., et al., 1990, ApJ 356, 160
Graf, U.U., Genzel, R., Harris, A.I., et al., 1990, ApJ 358 L49
Graf, U.U., Eckart, A., Genzel, R., et al., 1993, ApJ 405, 249
Haas, M.R., Hollenbach, D.J., Erickson, E.F., 1986, ApJ 301, 57

Hayashi, M., Hasegawa, T., Gatley, I., Garden, R., Kaifu, N., 1985, MNRAS 215, 31P
Hogerheijde, M.R., Jansen, D.J., van Dishoeck, E.F., 1994, Submillimeter Observations of Molecular Lines in the Orion Bar. In: Winnewisser, G. (ed.) Proc. Second Cologne-Zermatt Symposium (in press)
Icke, V., Gatley, I., Israel, F.P., 1980, ApJ 236, 808
Jansen, D.J., van Dishoeck, E.F., Black, J.H., 1994a, A&A 282, 605
Jansen et al., 1994b (Paper II) (in preparation)
Johnston, K.J., Palmer, P., Wilson, T.L., Bieging, J.H., 1983, ApJ 271, L89
Köster, B., Störzer, H., Stutzki, J., Sternberg, A., 1994, A&A 284, 545
Kutner, M.L., Ulich, B.L., 1981, ApJ 250, 341
Lacy, J.H., Knacke, R., Geballe, T.R., Tokunaga, A.T., 1994, ApJ Letters (in press)
Latter, W.B., Walker, C.K., Maloney, P.R., 1994, ApJ 419, L97
Le Bourlot, J., Pineau des Forêt, G., Roueff, E., Flower, D.R., 1993, A&A 267, 233
Mangum, J.G., Wootten, A., 1993, ApJS 89, 123
Martin, H.M., Sanders, D.B., Hills, R.E., 1984, MNRAS 208, 35
Meixner, M.M., Tielens, A.G.G.M., 1993, ApJ 405, 216
Omodaka, T., Hayashi, M., Hasegawa, T., 1984, ApJ 282, L77
Parmar, P.S., Lacy, J.H., Achtermann, J.M., 1991, ApJ 372, L25
Schloerb, F.P., Loren, R.B., 1982, Ann NY Ac Science, 395, 32
Spaans, M., 1994 (in preparation)
Stacey, G.J., Jaffe, D.T., Geis, N., et al., 1993, ApJ 404, 219
Sternberg, A., Dalgarno, A., 1989, ApJ 338, 197
Stutzki, J., Stacey, G.J., Genzel, R., Harris, A.I., Jaffe, D.T., 1988, ApJ 332, 379
Stutzki, J., Güsten, R., 1990, ApJ 356, 513
Tauber, J.A., Goldsmith, P.F., Dickmann, R.L., 1991, ApJ 375, 635
Tauber, J.A., Tielens, A.G.G.M., Meixner, M., Goldsmith, P.F., 1994, ApJ 422, 136
Tenorio–Tagle, G., 1979, A&A 7, 59
Tielens, A.G.G.M., Hollenbach, D., 1985a, ApJ 291, 722
Tielens, A.G.G.M., Hollenbach, D., 1985b, ApJ 291, 747
Tielens, A.G.G.M., Meixner, M.M., van der Werf, P.P., et al., 1993, Sci 262, 86
van Dishoeck, E.F., Black, J.H., 1988, ApJ 344, 711
van Dishoeck, E.F., Jansen, D.J., Phillips, T.G., 1993, A&A 279, 541
Wang, Y., Jaffe, D.T., Evans II, N.J., Hayashi, M., Tatematsu, K., Zhou, S., 1993, ApJ 419, 707
Werner, M.W., Gatley, I., Harper, D.A., et al., 1976, ApJ 204, 420
White, G.J., Padman, R., 1991, Nature 354, 511

This article was processed by the author using Springer-Verlag TEX A&A macro package 1992.